Image Reconstruction Using Wavelet Transform with Extended Fractional Fourier Transform

Prahallada Reddy Tammireddy

Rajesh Tammu

This thesis is presented as part of Degree of

Master of Science in Electrical Engineering

Blekinge Institute of Technology

June 2014

Blekinge Institute of Technology
Department of Applied Signal Processing
Supervisor: Ms Irina Gertsovich
Examiner: Dr. Sven Johansson

This thesis is submitted to the school of Engineering at Blekinge Institute of Technology in partial fulfilment of the requirements for the degree of Master of Science in Electrical Engineering. This thesis is equivalent to 20 weeks of full time studies

Contact Information

Authors:

Prahallada Reddy Tammireddy
E-mail: pralstpr@gmail.com

Rajesh Tammu
E-mail: rajesh.tammu@gmail.com

Supervisor:
Irina Gertsovich
Department of Applied Signal Processing
Blekinge Institute of Technology

Department of Applied Signal Processing

Blekinge Institute of Technology

371 79 KARLSKRONA

SWEDEN

Abstract

Image reconstruction forms the basis of many applications in the fields of medicine, astronomy etc. Historically an image is reconstructed using several methods of which Fourier and wavelet transform methods formed the roots of present day technologies. The reconstructed images possess higher resolution and helps in analysing the image in more detail. In our thesis we proposed a method where we used fractional Fourier transform in conjunction with wavelet transform to produce the reconstructed image. We employed three wavelets in our thesis namely Haar wavelet, Daubechies wavelet and Coiflet wavelet in order to gain diversity into our results. For the scaling function of each of the three wavelets fractional Fourier transform is applied which gives a new scaling function. A new wavelet function created using the scaling function. Such a wavelet is applied to series of images of various resolutions (256x256, 128x128, 64x64) and is encrypted using DES before transmitting over the channel. The reconstruction is carried out using inverse DES and inverse wavelet transform to get the reconstructed image.

The parameters we used to determine the efficiency of the wavelets are Peak Signal to Noise Ratio (PSNR) and Structural Similarity Index Metric (SSIM). The results for various images are plotted using box plots. We reached out the conclusions that Daubechies had the better performance compared to other wavelets. Also the performance falls down with the image resolution.

Keywords:

Wavelet Transform, Fourier Transform, Fractional Fourier Transform, Data Encryption Standards

Acknowledgements

We would like to express gratitude to our supervisor Ms Irina Gertsovich and examiner Dr. Sven Johansson for their excellent supervision and support throughout our thesis. Their guidance and encouragement has motivated us to accomplish our goal in research work.

We also want to thank all professors at the BTH who were part of our program who taught such thoughtful knowledge that aided us to finish our all courses and we also thank BTH for providing all the required amenities throughout our master's program.

We would like to thank God, our parents for their love and care and also our friends for inspiring and motivating us.

Table of Contents

List of Figures

Chapter 1: Background and Literature review

1.1 Background:

Image reconstruction is the process where in 2D or 3D images are constructed from set of 1D projections of an image [1]. It also includes the technique of developing a high resolution image from a set of low resolution images. In medicine, the magnetic resonance imaging and computerized tomography are used to scan the inner bodily functions of human body. Such applications require high resolution images but in early 20^{th} century highly focused images could not be generated due to limited technology of digital photography. These difficulties in the field of medicine gave birth to image reconstruction in early 20^{th} century since the Magnetic resonance imaging (MRI) or Computed Tomography (CT) data used in field of medicine must be visualized in detail.

The mathematical foundation for these reconstruction methods are the Radon transform [2], the inverse Radon transform [2], and the projection slice theorem [3]. Computational techniques include filtered back projection [4]. Several projection geometries are commonly used in medical applications including parallel beam, fan beam, and cone beam [5].

The first method was proposed by Johan Radon in 1917 in which the image is created based on the scattering data associated with cross sectional scans of an object [2]. Several methods of lesser or equal prominence were developed based on the Radon Transform over the course of time. In 1972 the first X- ray Computed Tomography (CT) was developed by Godfrey Hounsfield and the method served well in the field of medicine. The classical method of reconstruction is 'Back projection' [4] which is solely based on Radon transform. The alternate approaches include the basic Fourier Transform and wavelet transform methods.

In this thesis we concentrate on image reconstruction using wavelet methods. There are several goals with this thesis.

1) A possibility to employ wavelet transform with fractional Fourier transform for compression and reconstruction of an image with data encryption standards is investigated.

2) Which hybrid wavelets are efficient in the application of image reconstruction is assessed?

3) Performance of proposed method to reconstruct an image with hybrid wavelets is evaluated in terms of Structural Similarity Index Metric (SSIM) and Peak Signal to Noise Ratio (PSNR).

The thesis flow is described in the following way like Chapter 1 deals with background and literature review of the project. Chapter 2 deals with the theory, Chapter 3 deals with implementation of project and Chapter 4 is the analysis of results by examining the parameters. Finally Chapter 5 deals with conclusion and future work of the present work

1.2 Literature Review

Image reconstruction is an important aspect in the field of image processing. The quality of the reconstructed image should be high and therefore several algorithms are developed to achieve image reconstruction.

Algorithm to reconstruct the image has been developed by using partial 2D Fourier Transform [6]. In this algorithm authors have mainly concentrated on the bulk information accumulated across the four corners (blocks) of natural and aerial Fourier images. The frequency shift technique is applied to the sub blocks of images and the sub blocks are shifted in horizontal and vertical direction to map the data on four corners of image. To decompose and reconstruct the image Discrete Fourier Transform (DFT) and Inverse DFT are applied respectively. This method is requires low memory access and is computational less complex.

C.S. Tong and K.T. Leung have developed a super resolution reconstruction model based on linear interpolation of wavelet coefficients [7]. In this method, a high resolution image was reconstructed using a set of degraded, blurred and shifted low resolution images. They have used linear interpolation to build up an algorithm to obtain the relation between low resolution images and coefficients in wavelet sub bands. This method works even in the case of zero boundary conditions which eliminates need to specify the boundary conditions.

Y. Zhang, Y. Wang and C. Zhang have developed an algorithm to reconstruct a photo acoustic image by using Discrete Cosine Transform (DCT) [8]. In this method a calculated threshold value is set to remove the insignificant elements in DCT coefficients. An iterative formula is used to perform reconstruct image and iteration is repeated until the desired criteria is repeated. During reconstruction the optical deposition image and photo acoustic signals are processed separately. Due to the threshold value on DCT coefficients the reconstructed image will lose valuable data.

Another method to reconstruct image was developed by using Second Generation Wavelets (SGW) [9]. In this method image reconstruction is done by using set of significant data points. The significant data points are selected by using progressive significant sample point selection algorithm. In the approach to reconstruct image, the authors have used SGW and Delaunay triangulation to produce set of unique triangles and images. SGW possess the useful properties of wavelets like time-frequency localization, fast implementation and also capable to represent bounded domain signals.

In application required to reconstruct the missing blocks of an image, H.A. Azeez and S.A. Amin developed an algorithm to reconstruct medical image using wavelets and multi-wavelet methods [10]. In this Multi wavelets were formed with the aid of many filters and multi wavelets possess all the useful attributes of wavelets like symmetry, orthogonality and gives flexibility in the image reconstruction. This method depends on the average of high frequency elements surrounding the missing blocks and all the low frequency elements are assumed to be found.

Another method to reconstruct the missing blocks of an image was developed by H. Chen and I. Hagiwara [11]. To reconstruct the missing block of an image combination of wavelet decomposition, inpainting and texture synthesis methods are adopted. The input image is decomposed into high and low frequency components using wavelet decomposition algorithm. Multi resolution texture synthesis and compactly supported Radial basis functions are implemented on high frequency and low frequency components respectively to inpaint and modify the missing blocks. Inverse discrete wavelet transform algorithm is applied to reconstruct the image. Due to the inpainting, the boundary surrounding the reconstructed block changes significantly and the size of damaged area becomes wider.

The wavelet transforms served well for image reconstruction compared to that of Fourier transform because wavelets are descendants of the Fourier series. So all the drawbacks from the Fourier series are rectified in wavelets.

Fourier Transform is usually employed while working with a frequency domain. But Fourier Transform operates between integer values so some of the data in neglected while dealing with Fourier Transform. To overcome this we used a Fractional Fourier Transform (FrFT) which can be represented as some non-integer power. Also for encryption of electronic data we used basic Data Encryption Standard. So, In this thesis we employ Fractional Fourier Transform (FrFT) and Date Encryption Standard (DES) for the purpose of reconstructing an image

Chapter 2: Theory

2.1 Wavelet transforms

Wavelets are the functions of finite length and are oscillatory in nature. Wavelets are the localised vibrations of sound or images. In present world, wavelets have found a wide range of application in the field of signal processing such as image reconstruction and noise reduction. Wavelets can be used to reduce the size of an image without affecting the resolution of an image [12]. The mathematically representation of a wavelet is

$$\psi_{a,b}(t) = \frac{1}{\sqrt{a}}\psi\left(\frac{t-b}{a}\right) \ , \tag{2.1}$$

where a and b are scaling and shifting parameters, respectively.

Wavelet transforms can be operated easily by using fast wavelet transform. These wavelets are used in solving wide range of problems such as self-similarity property of a signal, signal discontinuities etc. Wavelet transforms are divided into 3 classes: Discrete wavelet transforms (DWT), Continuous wavelet transforms (CWT) and multi resolution based wavelet transform.

DWT works on two functions, namely scaling function and wavelet functions [13]. The analysis of signal at different scales is done by using the filters of different cut off frequencies. This decomposes the signal into different frequency bands, which are passed through the series of filters to analyse the high frequencies and low frequencies. CWT is a correlation between a wavelet and signal at different scales, where scale is used as a measure of similarity [14]. Multi resolution (MR) helps to study the signal at various frequencies with varying resolutions. MR offers better time resolution and poor frequency resolutions at high frequencies where as it offers better frequency resolution and poor time resolution at low frequencies. MR analysis is mostly applied when the signal contains low frequency components for long duration and high frequency components for small durations [13].

The wavelet transform of a function $f(t)$ is defined as [15, p44]

$$W(a,b) = \int_t f(t)\frac{1}{\sqrt{a}}\psi\left(\frac{t-b}{a}\right)dt \ , \tag{2.2}$$

The critical sampling of the CWT is obtained by taking $a = 2^{-j}$ and $b = ka$

$$W(j,k) = \int_t f(t)2^{\frac{j}{2}}\psi\left(2^j t - k\right)dt \ , \tag{2.3}$$

where j and k are integers representing the set of discrete translations and discrete dilation.

By substituting $a = 2^{-j}$ and $b = ka$ in Eq.2.1,

$$\psi_{j,k}(t) = 2^{\frac{j}{2}}\psi\left(2^{j}t - k\right). \tag{2.4}$$

If $j = 0\ and\ k = 0$, then $\psi_{0,0}(t) = \psi(t)$ which is considered as mother wavelet [15, p45].

The scaling function $\phi(t)$ is defined as[16][15, p66]

$$\phi(t) = \sum_{k\in z}\sqrt{2}h_k\phi(2t-k)\,, \tag{2.5}$$

where h_k is the filter coefficients in low pass filter (LPF) in a two-channel orthonormal wavelet system.

The wavelet function $\psi(t)$ is defined as [16][15, p66]

$$\psi(t) = \sum_{k\in z}\sqrt{2}g_k\phi(2t-k)\,, \tag{2.6}$$

where g_k is the filter coefficients in high pass filter (HPF) in a two-channel orthonormal wavelet system.

The LPF and HPF together constitute a pair of conjugate quadrature filters. i.e.,

$$g_k = (-1)^k h_{(k_1+k_2-k)}\,, \tag{2.7}$$

where $[k_1, k_2]$ is the support of FIR filters $h\ and\ g$.

The orthonormal condition is given by

$$\sum_{k\in z} h_k h_{(k-2n)} = \delta_n \tag{2.8}$$

for $n \in z$, where δ_n denotes the Kronecker delta symbol.

In this thesis, we will focus on 3 kinds of wavelets namely Haar wavelet [12], Daubechies wavelet [12] and Coiflets wavelet [18].

2.1.1 Haar wavelet

Haar wavelets [12] are the simplest form of wavelets available. Haar wavelet transform serves as prototype for all wavelet transforms. It can be used to compress signal and removing noise [12]. Haar transform y_n for n input function x_n can be estimated as:

$$y_n = H_n x_n \,, \tag{2.9}$$

where, H_n is Haar matrix and x_n is the n input function.

$$H_n = H_{2N} = \begin{bmatrix} H_N \otimes [1,1] \\ I_N \otimes [1,-1] \end{bmatrix}, \tag{2.9a}$$

where, I_N is identity matrix and $\otimes$ is kronecker product

Haar functions are orthogonal in nature which helps them to analyse the frequency components of the input signal. The length of input and output signal in a Haar transform should be equal.

Haar scaling function co-efficient [15, p65-66]

$$h_0 = \frac{1}{\sqrt{2}} \quad h_1 = \frac{1}{\sqrt{2}}$$

Haar scaling function

$$\phi(t) = h_0\sqrt{2}\,\phi(2t) + h_1\sqrt{2}\,\phi(2t-1). \tag{2.10}$$

Haar wavelet function co-efficient

$$g_0 = h_1 = \frac{1}{\sqrt{2}} \quad g_1 = -h_0 = -\frac{1}{\sqrt{2}}$$

Haar wavelet function

$$\psi(t) = g_0\sqrt{2}\,\phi(2t) + g_1\sqrt{2}\,\phi(2t-1). \tag{2.11}$$

2.1.2 Daubechies wavelet

Daubechies wavelet [12] was discovered by Ingrid Daubechies. Daubechies wavelets are compactly supported orthonormal wavelets [17]. These are the famous wavelet filters with certain limits these filters can produce a perfect reconstruction. Daubechies wavelet consists of different kinds of wavelets, such as Db4 (Daubechies 4 wavelet), Db6, Db8 and so on to

Db20. Db4 is the simplest wavelet among the Daubechies wavelet series. Db4 is one of the method which deals with edges of finite periodic data sets [13].

The Db4 scaling and wavelet function co-efficient are given by[15, p79].

Db4 scaling function co-efficient

$$h_0 = \frac{1+\sqrt{3}}{4\sqrt{2}} \quad h_1 = \frac{3+\sqrt{3}}{4\sqrt{2}} \quad h_2 = \frac{3-\sqrt{3}}{4\sqrt{2}} \quad h_3 = \frac{1-\sqrt{3}}{4\sqrt{2}}$$

Db4 scaling function

$$\phi(t) = h_0\sqrt{2}\,\phi(2t) + h_1\sqrt{2}\,\phi(2t-1) + h_2\sqrt{2}\,\phi(2t-2) + h_3\sqrt{2}\,\phi(2t-3). \quad (2.12)$$

Db4 wavelet function co-efficient

$$g_0 = h_3 = \frac{1-\sqrt{3}}{4\sqrt{2}} \quad g_1 = -h_2 = \frac{-3+\sqrt{3}}{4\sqrt{2}} \quad g_2 = h_1 = \frac{3+\sqrt{3}}{4\sqrt{2}} \quad g_3 = -h_0 = \frac{-1-\sqrt{3}}{4\sqrt{2}}$$

Db4 wavelet function

$$\psi(t) = g_0\sqrt{2}\,\phi(2t) + g_1\sqrt{2}\,\phi(2t-1) + g_2\sqrt{2}\,\phi(2t-2) + g_3\sqrt{2}\,\phi(2t-3). \quad (2.13)$$

2.1.3 Coiflets wavelet

Coiflets wavelets were built by Ingrid Daubechies at the request of Ronald Coifman. Coiflets wavelet belongs to the family of orthogonal wavelet. For the efficient implementation these filters are compactly supported corresponding to finite impulse response filters. For both scaling and wavelet functions these wavelets have high number of vanishing moments when supported compactly. There are 2N moments of wavelet functions which are equal to zero and 2N-1 moments of scaling functions which are equal to zero [18]. Coiflets consists of different kinds of wavelets such as coif6 (Coiflets 6 wavelet), coif12 and so on to coif20.

The Coif6 scaling and wavelet function co-efficient are given by

Coif6 scaling function co-efficient

$$h_0 = \frac{1-\sqrt{7}}{16\sqrt{2}} \quad h_1 = \frac{5+\sqrt{7}}{16\sqrt{2}} \quad h_2 = \frac{14+2\sqrt{7}}{16\sqrt{2}} \quad h_3 = \frac{14-2\sqrt{7}}{16\sqrt{2}}$$

$$h_4 = \frac{1-\sqrt{7}}{16\sqrt{2}} \quad h_5 = \frac{-3+\sqrt{7}}{16\sqrt{2}}$$

Coif6 scaling function

$$\phi(t) = h_0\sqrt{2}\,\phi(2t) + h_1\sqrt{2}\,\phi(2t-1) + h_2\sqrt{2}\,\phi(2t-2) + h_3\sqrt{2}\,\phi(2t-3) + h_4\sqrt{2}\,\phi(2t-4) + h_5\sqrt{2}\,\phi(2t-5). \quad (2.14)$$

Coif6 wavelet function co-efficient

$$g_0 = h_5 = \frac{-3+\sqrt{7}}{16\sqrt{2}} \quad g_1 = -h_4 = \frac{-1+\sqrt{7}}{16\sqrt{2}} \quad g_2 = h_3 = \frac{14-2\sqrt{7}}{16\sqrt{2}}$$

$$g_3 = -h_2 = \frac{-14-2\sqrt{7}}{16\sqrt{2}} \quad g_4 = h_1 = \frac{5+\sqrt{7}}{16\sqrt{2}} \quad g_5 = -h_0 = \frac{-1+\sqrt{7}}{16\sqrt{2}}$$

Coif6 wavelet function

$$\psi(t) = g_0\sqrt{2}\,\phi(2t) + g_1\sqrt{2}\,\phi(2t-1) + g_2\sqrt{2}\,\phi(2t-2) + g_3\sqrt{2}\,\phi(2t-3) + g_4\sqrt{2}\,\phi(2t-4) + g_5\sqrt{2}\,\phi(2t-5). \quad (2.15)$$

2.2 Fractional Fourier transform

The fractional Fourier transform (FrFT) is the generalized form of Fourier transform (FT) which relies on order parameter a [19]. The FrFT with $a = 0$ is the identity operator and $a = 1$ is the normal Fourier transform operator. FrFT has found many applications in signal processing, image processing, communications and wave propagation [19][20]. The a^{th}order FrFT is the a^{th} power of ordinary FT. For an intermediate value, fractional angle α $\left(0 < \alpha < \frac{\pi}{2}\ or\ 0 < \alpha < 1\right)$ produces a rotated signal representation of time frequency domain. If FT is denoted by F then the a^{th} order FrFT is denoted by F^a. The zero order FrFT can be denoted by F^0, the F^0 of function $f(t)$ will be equal to the function itself. The first order FrFT can be denoted by F^1. First order FrFT of function $f(t)$ will be equal to the Fourier transform $F(\mu)$ where μ is frequency domain variable. The inverse of first order FrFT can be denoted as F^{-1}. FrFT contain identical Eigen functions as that of normal FT whereas eigenvalues are raised to power of fraction [19].

The a^{th} order FrFT of the function $f(t)$ is denoted by $f_a(u)$ and defined as

$$f_a(u) = \int_{-\infty}^{\infty} K_a(t,u) f(t) dt\,, \quad (2.16)$$

where the kernel $K_a(t,u) = A_\alpha e^{[i\pi(\cot(\alpha t^2) - 2\csc(\alpha t u) + \cot(\alpha u^2))]}$, (2.16a)

where $A_\alpha = \sqrt{1 - icot\alpha}$ and $\alpha = \frac{a\pi}{2}$.

The cot and cosec function in the above equations deviates if a is an integer multiple of π.

If $a = 4j$ then

$$K_a(t,u) = \delta(t-u).$$

If $a = 4j + 2$ then

$$K_a(t,u) = \delta(t+u).$$

When $a \neq 2j$, the kernel $K_a(t,u)$ approaches to a delta function

The a' order transform of a^{th} order FT will be equivalent to $(a' + a)^{th}$ order FT [21]. If the F^a is periodic with period $a = 4$, then $F^a = F^{a+4j}$ where a is assumed to be real value and j is integer. The operator F^2 is equal to parity operator P which maps $f(t)$ to $f(-t)$ and the operator F^4 is equal to identity operator. The range of a is confined to $(-2,2]\ or\ [0,4)$ [21].

Applications of FrFT can be found in optimal information processing area. FrFT generalize the concepts of time and frequency domains which results in many application in the field of signal processing [19].

2.3 Data Encryption Standards

Data Encryption Standards was set up by International Business Machines (IBM) as a research project in late 1960's [22]. The result of the project was a cipher known as LUCIFER. Many significant changes were introduced into LUCIFER before commercializing in 1970's. IBM seeks technical help from National Security Agency (NSA) to implement the changes in LUCIFER. In 1977 LUCIFER was accepted as new national encryption standards by National Bureau of Standards (NBS). Even to present day, there exists a controversy on the changes made to LUCIFER and the most notable was key size [22].

DES encrypts 64 bit data at a time as the block cipher used is of 64bits. Even though DES accepts 64 bits key, we just use 56 bits as input and the rest 8 bits have no effect on DES security and used for parity check. In each byte the least significant bit is used for parity check and does not helps to increase the security standards [23].

The DES encryption and decryption principles [23] are shown in fig 2.1.

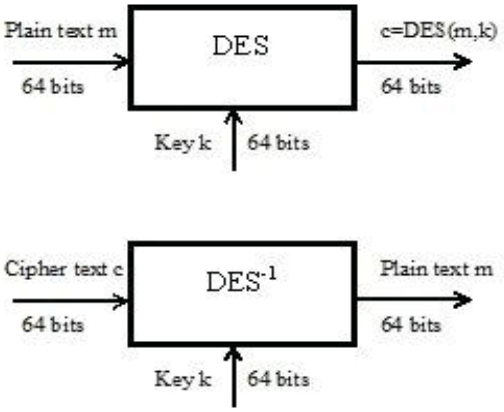

Fig2.1: DES Encryption and Decryption Algorithm

The flowchart of the DES encryption algorithm [23] is shown in fig 2.2.

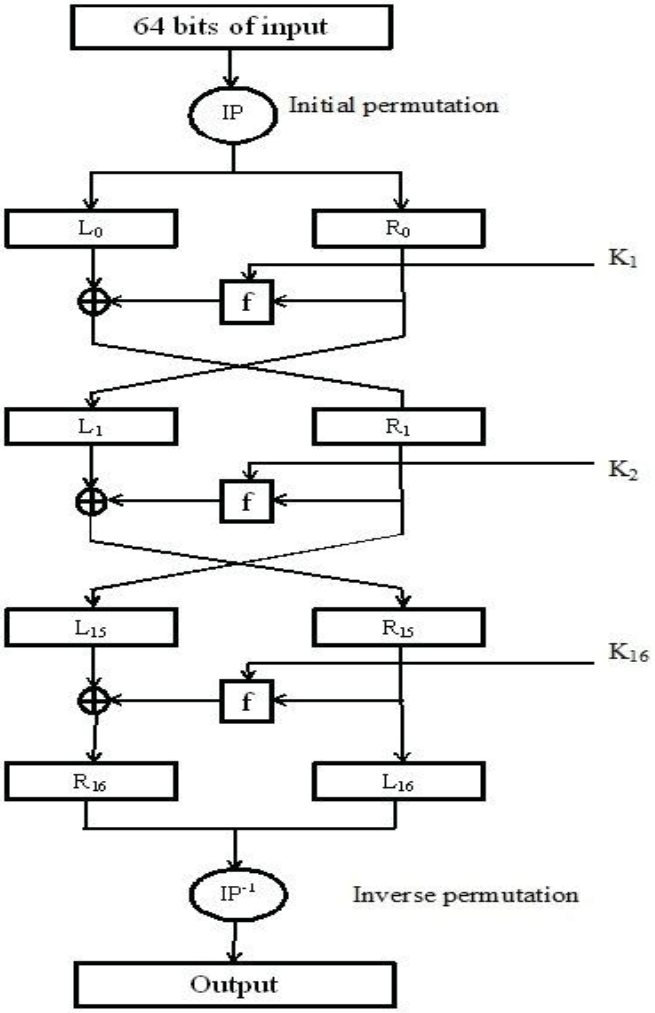

Fig2.2: DES Encryption Algorithm

Working Principle

Once the message to be sent is received, it is rearranged into blocks of 64 bits. The message received is mapped among the 64 bits. If any of the bits are unoccupied then the zeros will be padded. The initial permutations is performed on these 64 bit data and these bits are split into two groups of each 32 bit sub blocks L_i and R_i. Next these sub blocks are processed in 16 rounds. Each round is identical and effects in increasing sub blocks number in two-fold. Sub blocks are passed through 16 rounds to eliminate correlation between the plain text and cipher text. The 32 bit L_i and R_i are swapped at the end of 16^{th} round to create a pre-output. The pre-output is finally permutated with the exact inverse of the initial permutation to receive the 64 bit cipher text [22]. DES decryption is an exact inverse of DES encryption process.

2.3.1 Key Schedule

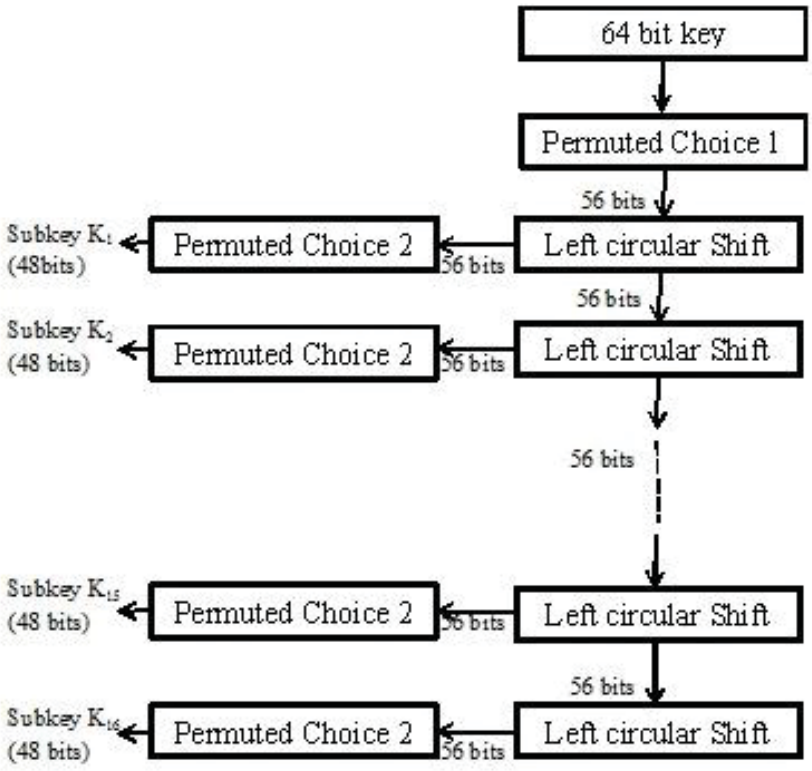

Fig 2.3: Key schedule of DES

Fig 2.3 shows the key schedule of DES. In key scheduling 48-bits of key is obtained from the original 56-bit key. The 48-bit sub key is an input to the Feistel function block happening in each round of DES encryption. Initially a 56-bits are chosen from the 64-bit data by performing a Permuted choice 1(PC-1) and the rest 8-bits are used for parity check. Now the 56-bit key is split into two halves of 28-bits each. These 28-bits are treated separately and

shifted simply by left cyclic shift for once or twice depending upon the round number. The Left cyclic shifted 28-bits of two halves are given as a input to Permuted choice 2(PC-2). The PC-2 produces 48-bits sub key as an output which is given as input to Feistel function in each round [22].

2.3.2 Feistel function

Feistel function is the main operation performed in each round of DES encryption algorithm. A Feistel function accepts 32-bit and 48-bit data as an input and produces a single 32-bit output. Feistel function consists of four stages namely Expansion, key mixing, substitution and permutation. Fig 2.4 shows the stages Feistel function

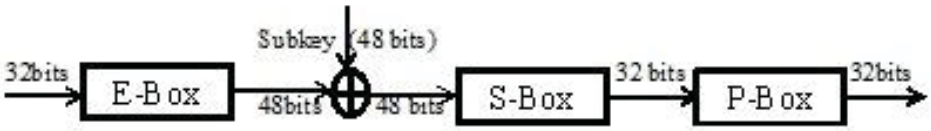

Fig 2.4: Feistel function

E-box Expansion

In this stage the 32-bit input for each round is expanded and permuted to give 48-bits necessary for combination with 48-bit key. The 32-bit input is converted into 48-bits by splitting its inputs into eight 4-bit blocks. Now the first and fourth bit of each 4-bit block is copied into the output in a defined manner along with 4-bit blocks. This results in 48-bits spitted into eight 6-bit blocks [22].

Key mixing

The 48-bits obtained in an expansion stage is combined with 48-bit sub key with the help of X-OR. The 48-bit sub key is derived from 56-bit key through key schedule [22].

S-box Substitution

The S-box substitution accepts 48-bits as input and produces the 32-bit output. In S-box substitution we have 8 S-boxes; each S-box accepts only 6-bit blocks. The 48-bit block is split into eight 6-bit blocks and fed to S-boxes. The output of an each S-box is a four bit block which results in 32-bits of eight 4-bit blocks [22].

P-box Permutation

The 32-bit output of an S-box is simply permutated without changing the size of data. The P-box maps one to one on input to output resulting in an output of 32-bit from the input of 32-bits [22].

2.4 Quality Measurement

The criteria's used to measure the performance index of image compression are objective fidelity criteria and subjective fidelity criteria.

2.4.1 Mean Square Error (MSE)

MSE is a one of the quality measurement parameter belonging to objective fidelity criteria. MSE gives an average estimate of the energy lost in the lossy compression of the original image. If the two images are consider to be affected by the same type of degradation, and then the image with smaller MSE will be closer to the original image. However the MSE has some problems when images with different types of degradations are compared.

The mean square error between the original image and the reconstructed image is given by

$$MSE = \frac{1}{M \times N} \sum_{m=0}^{M-1} \sum_{n=0}^{N-1} \big(f(m,n) - g(m,n)\big)^2 , \tag{2.17}$$

where $f(m,n)$ is original image, $g(m,n)$ is reconstructed image and $M \times N$ is size of an image [24].

2.4.2 Peak Signal to Noise Ratio (PSNR)

Peak Signal to Noise Ratio (PSNR) is an objective quality measurement of distortion. PSNR uses a constant value to compare the noise against the fluctuating signal used in Signal to Noise Ratio (SNR). Due to this reason the values received from the PSNR are treated more meaningfully when compared with different image coding algorithms [24]. The unit of PSNR is dB (decibel).

PSNR is defined as

$$PSNR = 10 \log_{10} \left[\frac{\left(2^b - 1\right)^2}{MSE} \right] \ dB. \tag{2.18}$$

For an 8 bit image, $b = 8$ then

$$PSNR = 10 \log_{10} \left[\frac{(255)^2}{MSE} \right] \ dB. \tag{2.19}$$

2.4.3 Structural Similarity Index Metric (SSIM)

SSIM is an alternative method to evaluate the perceptual quality of an image. SSIM is an objective image quality assessment metric used to predict the image quality. SSIM measures the structural similarity between the two frames of original and reconstructed image. SSIM takes the quality degradations from the structural information by comparing two frames [25]. SSIM is defined as

$$SSIM(x,y) = \frac{(2\mu_x\mu_y + C_1)(2\sigma_{xy} + C_2)}{(\mu_x^2 + \mu_y^2 + C_1)(\sigma_x^2 + \sigma_y^2 + C_2)}, \tag{2.20}$$

where μ_x and μ_y are the mean of x and y respectively, σ_x^2 and σ_y^2 are the variance of x and y respectively, σ_{xy} is the co-variance of x and y. $C_1 = (k_1 L)^2$ and $C_2 = (k_2 L)^2$ are the constants used to avoid instabilities in the structural similarity comparison [25].

where L is dynamic range of pixel values, $k_1 = 0.01 \; and \; k_2 = 0.03$ by default.

The Mean SSIM (MSSIM) index is defined as

$$MSSIM(X, Y) = \frac{1}{M} \sum_{j=1}^{M} SSIM\left(x_j, y_j\right), \tag{2.21}$$

where M is number of local windows in image [25].

Chapter 3: Implementation

In this chapter, we will discuss about the step by step implementation procedure used in this thesis. The block diagram of implementation procedure is shown in fig 3.1

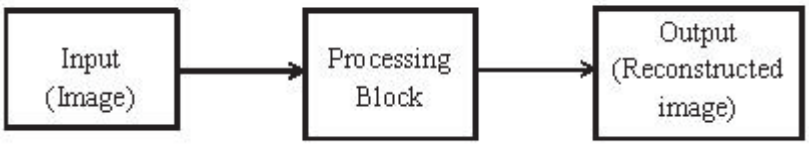

Fig 3.1: Block diagram of implementation procedure

3.1 Input

The bio-medical grey scale image of 256x256 pixel resolution is selected as an input to the wavelet transform in this thesis.

3.2 Processing Block

The processing block consists of various stages which are shown in fig 3.2 and explained in section 3.2.1 to 3.2.9.

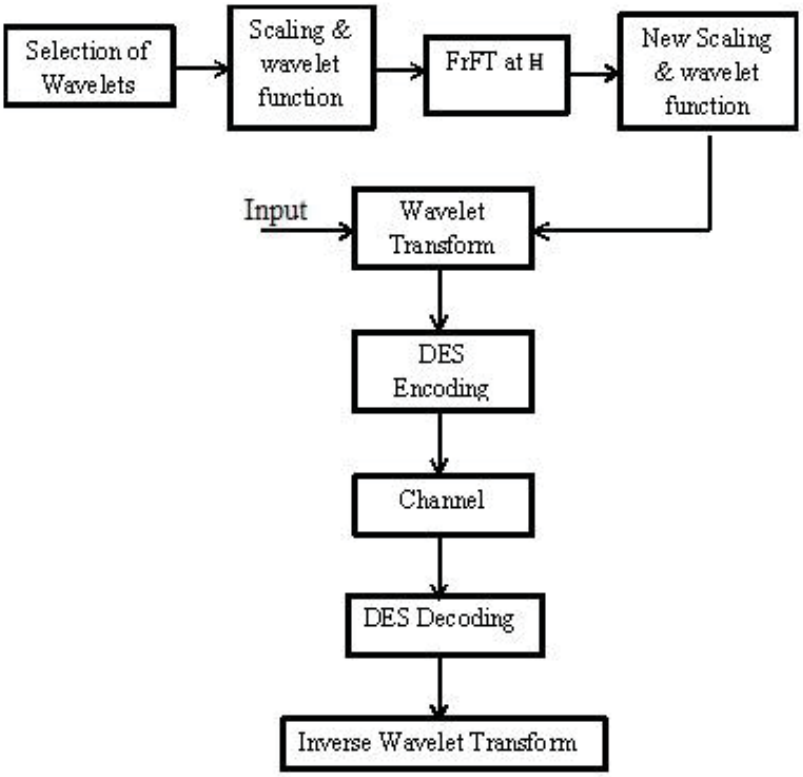

Fig 3.2: Flowchart of processing bock

3.2.1 Selection of wavelets

In this step we will consider 3 wavelets namely Haar wavelet, Daubechies wavelet and Coiflets wavelet. We have chosen Haar wavelet because Haar wavelet is the simplest form of wavelets available [12]. Daubechies wavelet is chosen because Daubechies wavelets are compactly supported orthonormal wavelets [17]. Coiflets wavelets are chosen as there are 2N moments of wavelet functions which are equal to zero and 2N-1 moments of scaling functions which are equal to zero [18].

3.2.2 Scaling and wavelet function of wavelet

We summarize the scaling and wavelet functions below.

Haar scaling function

$$\phi(t) = \left[\frac{1}{\sqrt{2}} \quad \frac{1}{\sqrt{2}}\right]$$

Haar wavelet function

$$\psi(t) = \left[\frac{1}{\sqrt{2}} \quad \frac{-1}{\sqrt{2}}\right]$$

Db4 scaling function

$$\phi(t) = \left[\frac{1+\sqrt{3}}{4\sqrt{2}} \quad \frac{3+\sqrt{3}}{4\sqrt{2}} \quad \frac{3-\sqrt{3}}{4\sqrt{2}} \quad \frac{1-\sqrt{3}}{4\sqrt{2}}\right]$$

Db4 wavelet function

$$\psi(t) = \left[\frac{1-\sqrt{3}}{4\sqrt{2}} \quad \frac{-3+\sqrt{3}}{4\sqrt{2}} \quad \frac{3+\sqrt{3}}{4\sqrt{2}} \quad \frac{-1-\sqrt{3}}{4\sqrt{2}}\right]$$

Coif6 scaling function

$$\Phi(t) = \left[\frac{1-\sqrt{7}}{16\sqrt{2}} \quad \frac{5+\sqrt{7}}{16\sqrt{2}} \quad \frac{14+2\sqrt{7}}{16\sqrt{2}} \quad \frac{14-2\sqrt{7}}{16\sqrt{2}} \quad \frac{1-\sqrt{7}}{16\sqrt{2}} \quad \frac{-3+\sqrt{7}}{16\sqrt{2}}\right]$$

Coif6 wavelet function

$$\psi(t) = \left[\frac{-3+\sqrt{7}}{16\sqrt{2}} \quad \frac{-1+\sqrt{7}}{16\sqrt{2}} \quad \frac{14-2\sqrt{7}}{16\sqrt{2}} \quad \frac{-14-2\sqrt{7}}{16\sqrt{2}} \quad \frac{-5-\sqrt{7}}{16\sqrt{2}} \quad \frac{1-\sqrt{7}}{16\sqrt{2}}\right]$$

3.2.3 Fractional Fourier transforms (FrFT)

In this stage we vary the scaling function and wavelet function of a selected wavelet by using FrFT. To vary the scaling and wavelet function, we should select the fractional angle α $(0 < \alpha < 1)$ at which FrFT would occur.

The FrFT of the wavelet is denoted by $X_\alpha(u)$ and is defined as follows

$$X_\alpha(u) = \int_{-\infty}^{\infty} \psi_{a,b}(t)\, K_\alpha(t,u) dt\,. \tag{3.1}$$

$X_\alpha(u)$ is the new wavelet that depends on the fractional angle α and $K_\alpha(t,u)$ is defined in Eq.2.16a.

3.2.4 New wavelet

After modulating the scaling and wavelet function by using FrFT we get the wavelet family with new scaling and wavelet function which is considered as new wavelet. Even after modification, the new wavelet kernel remains same as kernel of old wavelet transform. For every wavelet we selected at the initial stage we get a family of new wavelet after performing FrFT. As we vary the fractional angle a the scaling and wavelet function get altered which results in a family of wavelet which are unique from one another.

3.2.5 Wavelet transform

In this step, the wavelet transform is performed on the input image $w(t)$ by means of the newly obtained scaling and wavelet function. The wavelet transform for the new wavelet is defined as follows

$$W(a,b)_\alpha = \int_t w(t)\, X_\alpha(u)\mathrm{dt} \tag{3.2}$$

The data obtained after the wavelet transform is subjected to DES encryption.

3.2.6 DES Encoding

The data obtained from the wavelet transformation is encoded with DES. For more information about DES encoding refer to section 2.3.

3.2.7 Channel

In this stage the data encoded with DES is passed through the channel, for example, in a bio-medical case a data is sent from ambulance to hospital.

3.2.8 DES Decoding

The code received from a channel is decoded by using the DES decryption process. DES decryption is an exact inverse of a principle happening in a DES encryption process.

3.2.9 Inverse Wavelet Transform (IWT)

In this stage the signal in complex plane is converted into a signal in time domain by using IWT. IWT is an exact inverse of process happening in wavelet transform.

Inverse wavelet transform is defined as

$$w(t) = \int_a \int_b \frac{1}{a^2} W(a,b)_\alpha X_\alpha(u)\, da\, db \tag{3.3}$$

3.3 Output

After performing the inverse wavelet transform the reconstructed image is obtained. The performance of a reconstructed image is checked by using the parameters Peak Signal to Noise Ratio (PSNR) and Structural Similarity Index Metric (SSIM). For more details about PSNR and SSIM refer to section 2.4.

Chapter 4: RESULTS

4.1 Results

4.1.1 Input image

Let us consider the image of 256x256 pixels in Fig 4.1 as an input image.

Fig 4.1: Input image

4.1.2 Original Scaling and wavelet functions

Fig 4.2 shows the plot of scaling and wavelet functions of the wavelets.

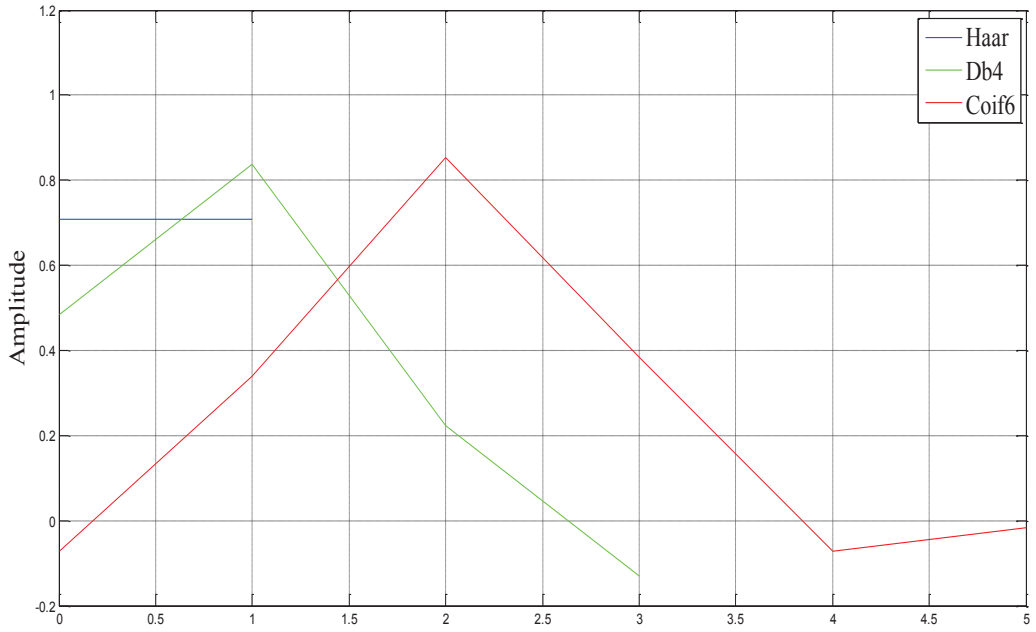

(a)

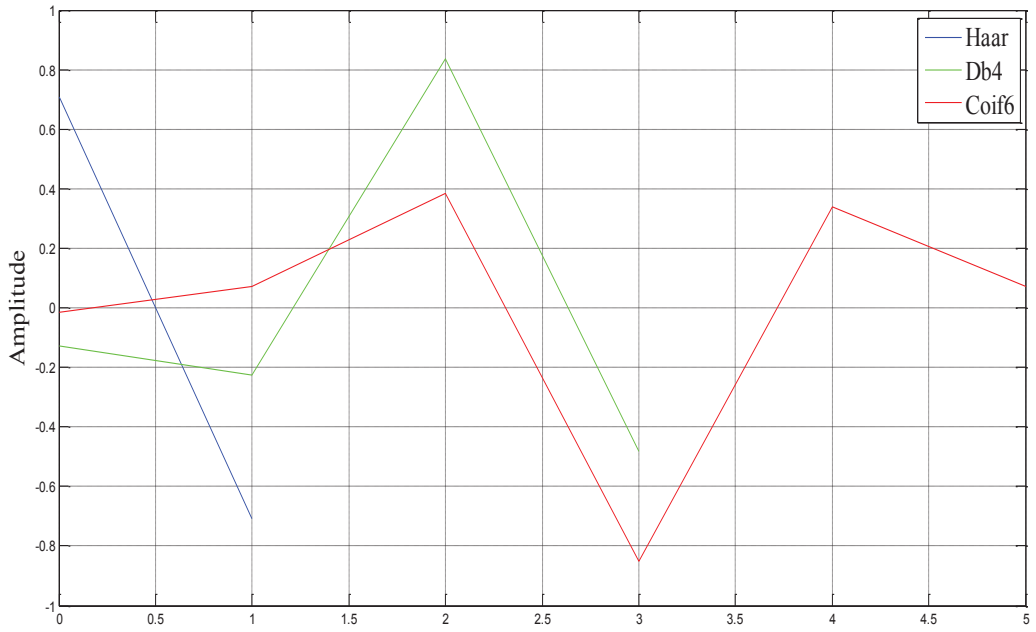

(b)

Fig 4.2: a) Scaling and b) wavelet functions of Haar, Daubechies 4 and Coiflet 6 wavelets.

The magnitudes and phases of frequency response functions (scaling function) for Haar, Daubechies 4 and Coiflet 6 wavelets are shown in Fig 4.3 and 4.4, respectively

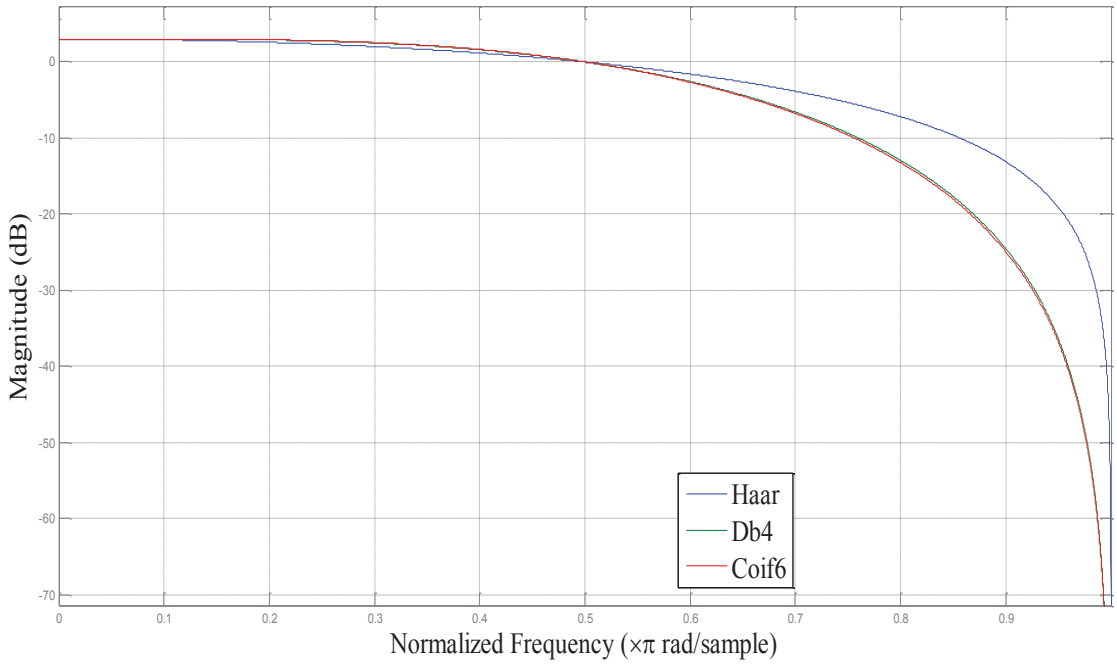

Fig 4.3: Magnitudes of frequency response functions for Haar, Daubechies 4 and Coiflet 6 wavelets.

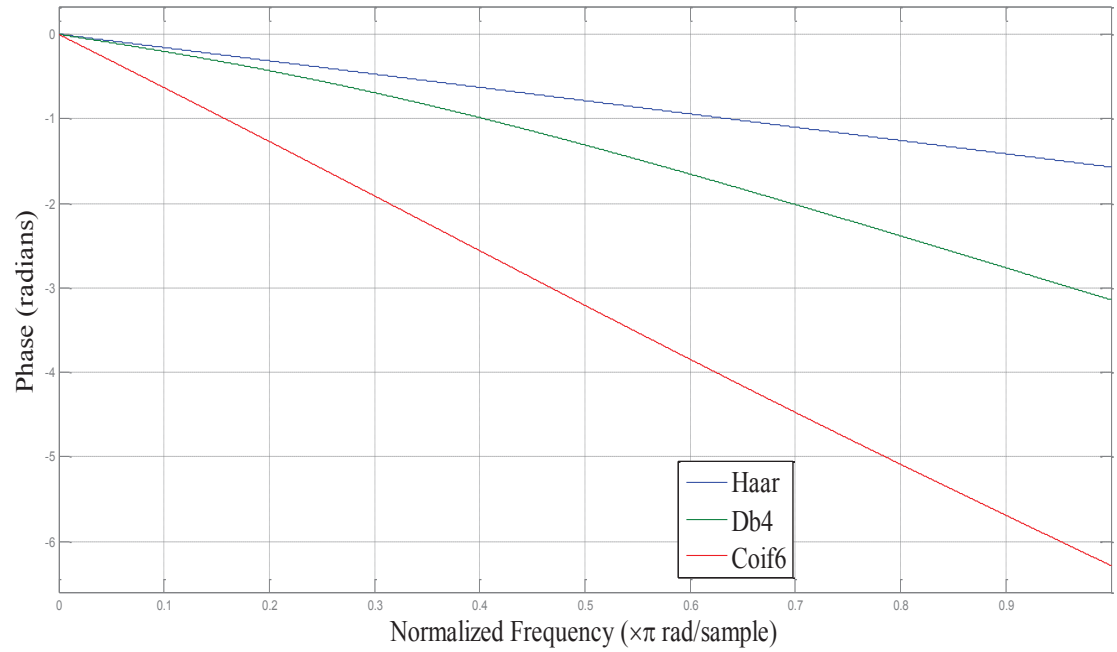

Fig 4.4: Phases of frequency response functions for Haar, Daubechies 4 and Coiflet 6 wavelets.

The magnitudes and phases of frequency response functions (wavelet function) for Haar, Daubechies 4 and Coiflet 6 wavelets are shown in Fig 4.5 and 4.6, respectively

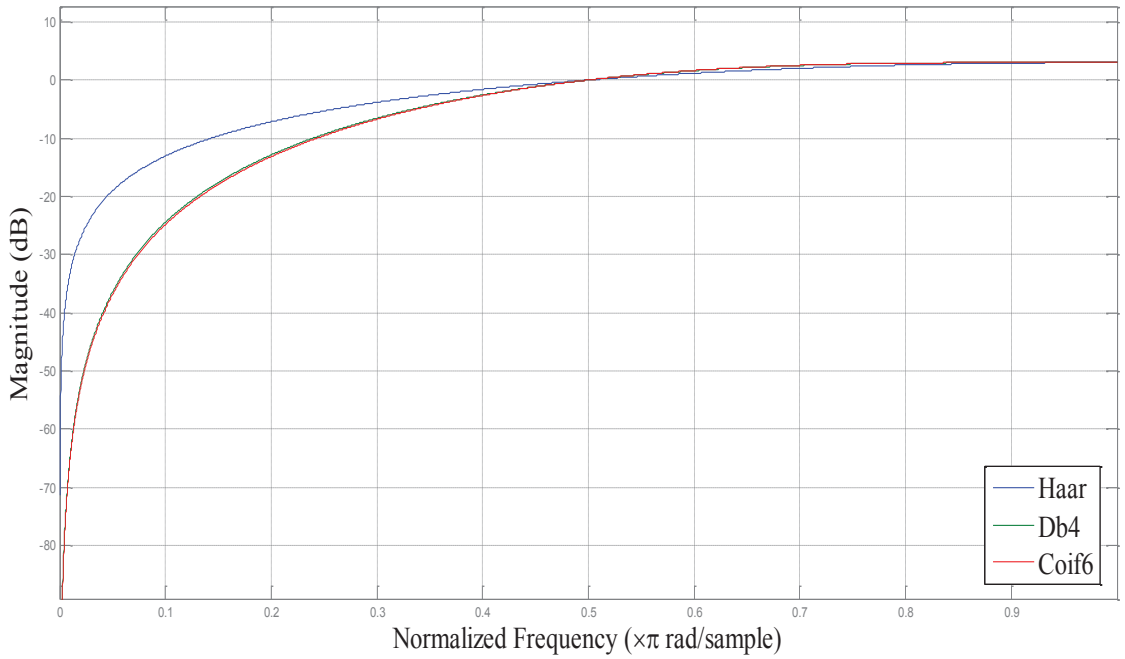

Fig 4.5: Magnitudes of frequency response functions for Haar, Daubechies 4 and Coiflet 6 wavelets.

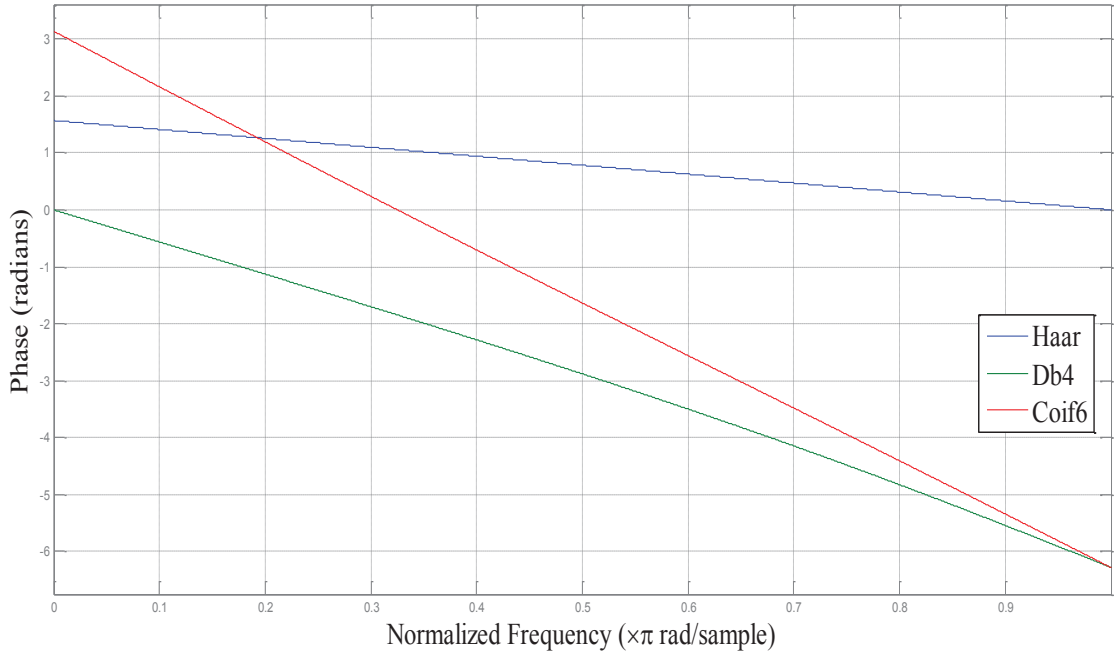

Fig 4.6: Phases of frequency response functions for Haar, Daubechies 4 and Coiflet 6 wavelets.

To demonstrate effect of the fractional angle of FrFT on the scaling and wavelet functions we calculate the hybrid scaling and wavelet functions for fractional angle $\alpha = 0.2$ according Eq. 3.1. The coefficients of the hybrid scaling function are shown in Fig 4.7 a) and the hybrid wavelet function based on these coefficients is shown in Fig 4.7 b)

4.1.3 Scaling function and wavelet function with extended FrFT

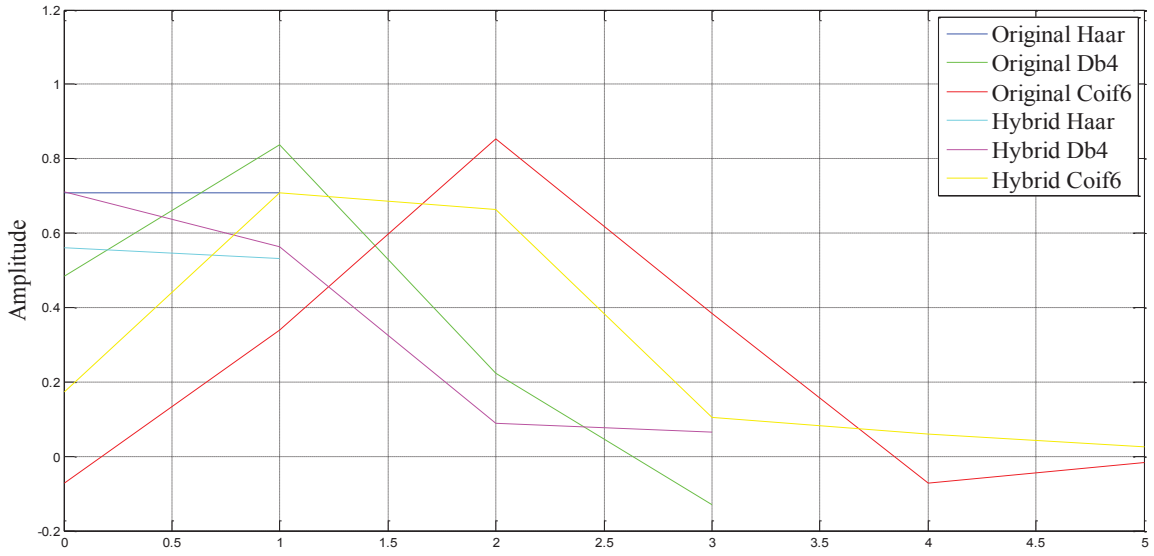

(a)

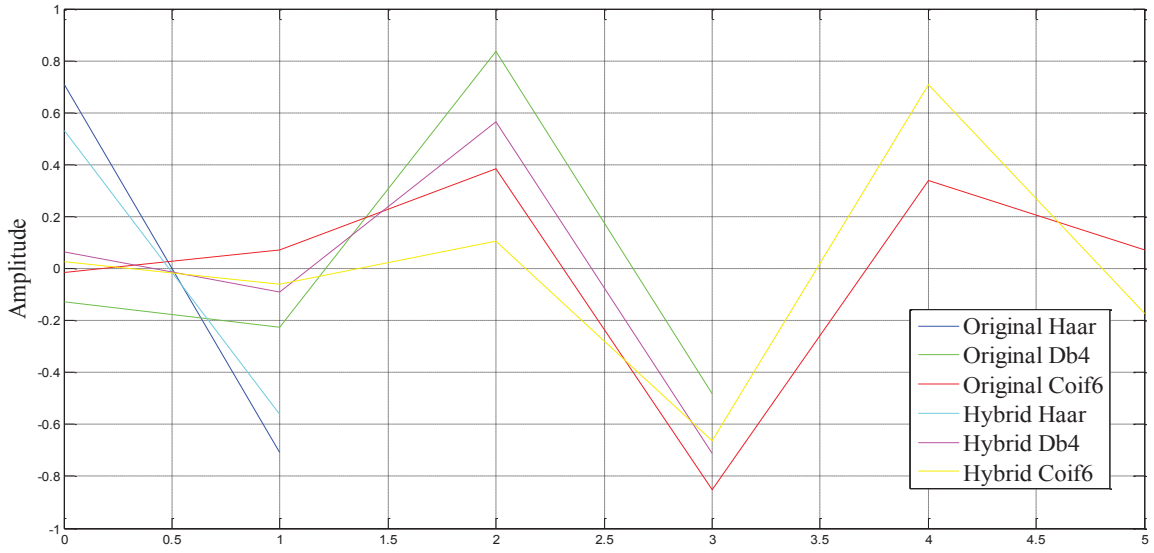

(b)

Fig 4.7: a) Scaling and b) wavelet functions of original and hybrid Haar, Daubechies 4, Coiflet 6 wavelets.

The magnitudes and phases of frequency response functions (scaling function) for original and hybrid Haar, Daubechies 4 and Coiflet 6 wavelets are shown in Fig 4.8 and 4.9, respectively

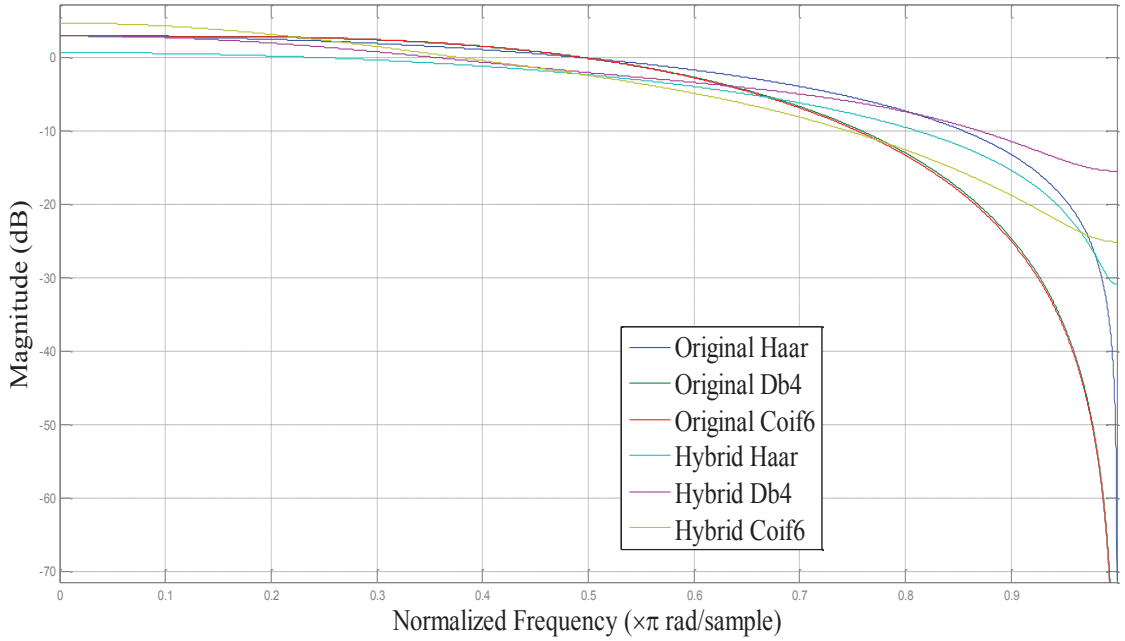

Fig 4.8: Magnitudes of frequency response functions for original and hybrid Haar, Daubechies 4 and Coiflet 6 wavelets.

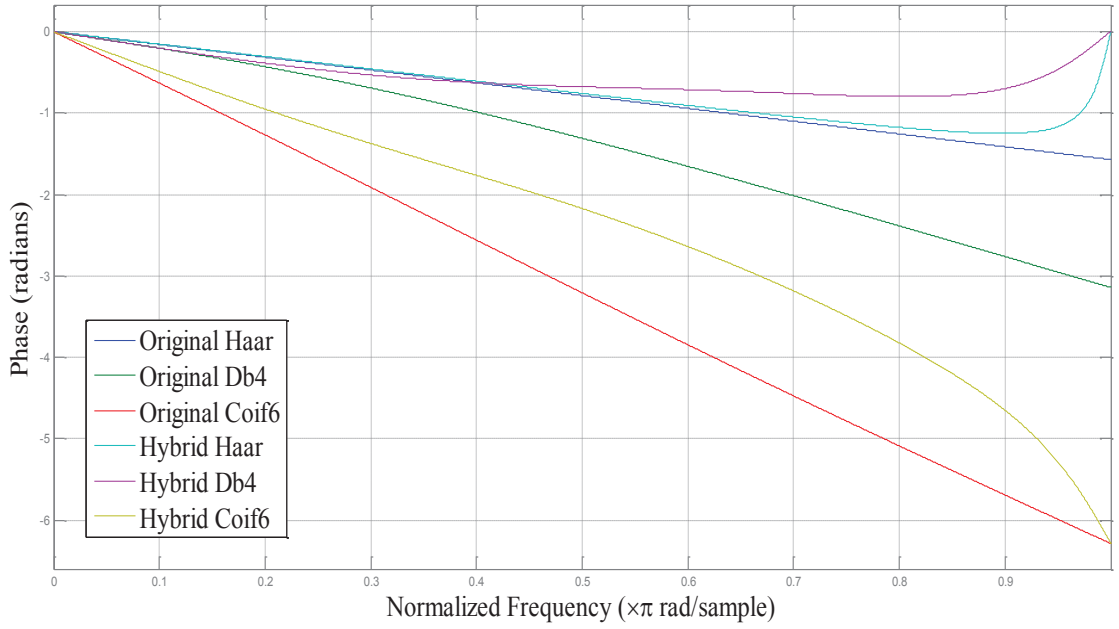

Fig 4.9: Phases of frequency response functions for original and hybrid Haar, Daubechies 4 and Coiflet 6 wavelets.

The magnitudes and phases of frequency response functions (wavelet function) for original and hybrid Haar, Daubechies 4 and Coiflet 6 wavelets are shown in Fig 4.10 and 4.11, respectively

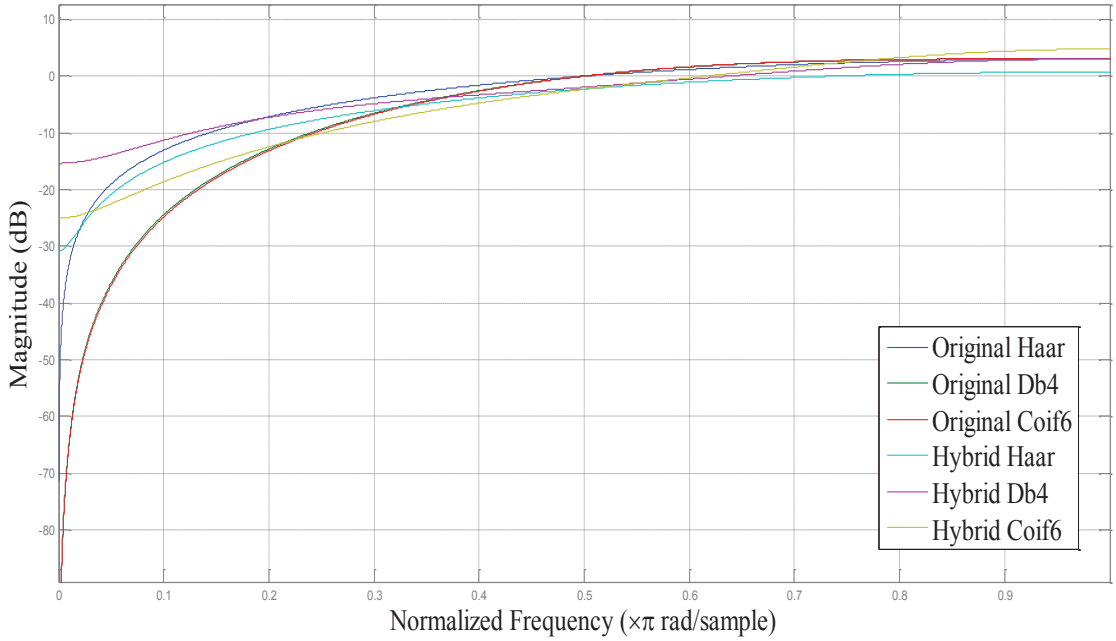

Fig 4.10: Magnitudes of frequency response functions for original and hybrid Haar, Daubechies 4 and Coiflet 6 wavelets.

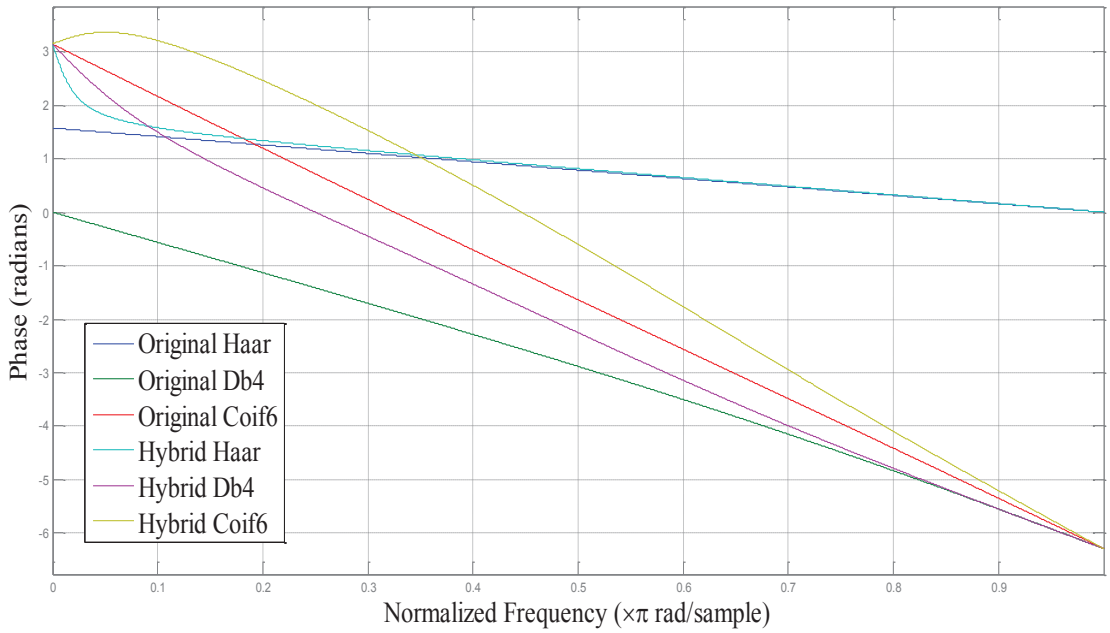

Fig 4.11: Phases of frequency response functions for original and hybrid Haar, Daubechies 4 and Coiflet 6 wavelets.

4.1.4 Decomposition of image using hybrid wavelets

The result of the decomposition of an image using Haar, Daubechies 4 and Coiflet 6 hybrid wavelets is shown in Fig 4.12 a), Fig 4.12 b), Fig 4.12 c) respectively.

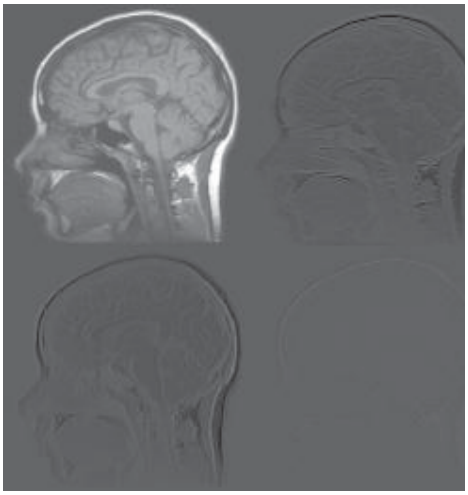

(a)

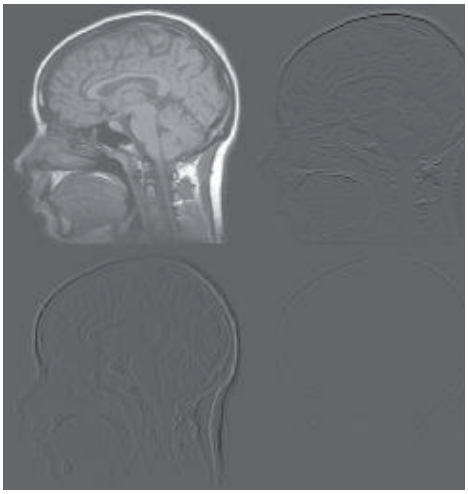

(b)

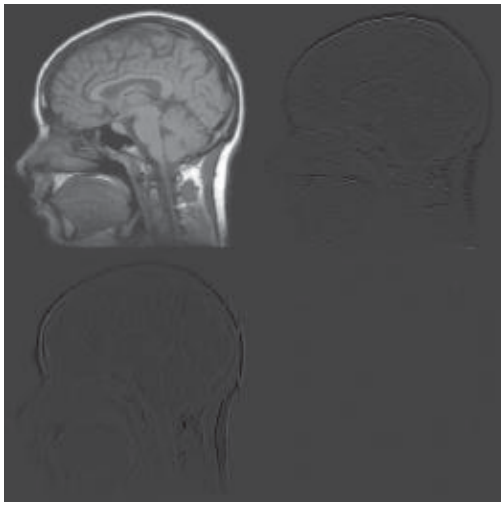

(c)

Fig 4.12: Decomposition of an image using hybrid (a) Haar wavelet, (b) Daubechies 4 wavelet, (c) Coiflet 6 wavelet.

4.1.5 Reconstruction of original image using decomposed images

The result of the reconstructed image using Haar, Daubechies 4 and Coiflet 6 hybrid wavelets is shown in Fig 4.13 a), Fig 4.13 b), Fig 4.13 c) respectively.

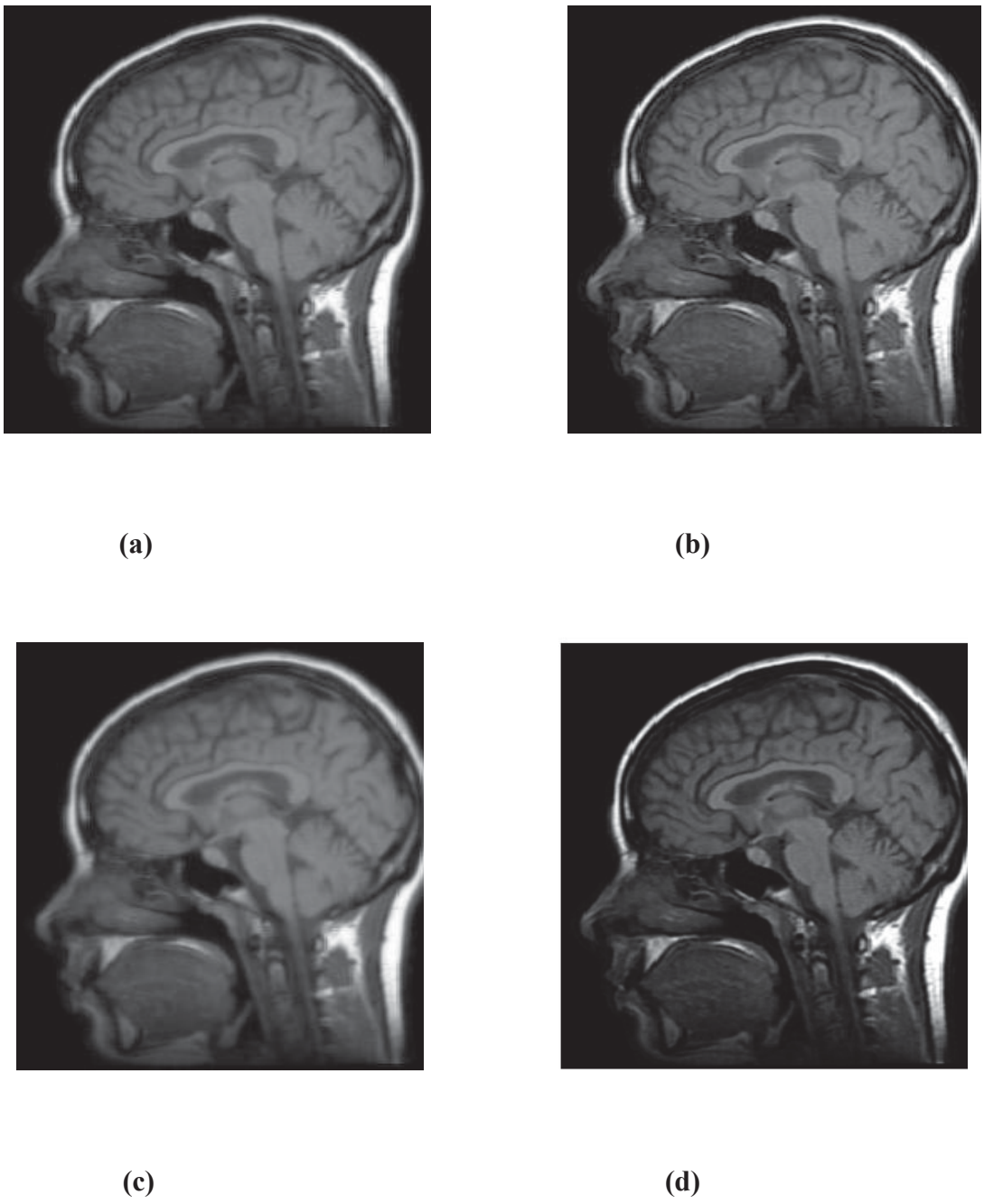

(a) **(b)**

(c) **(d)**

Fig 4.13: Reconstructed image using (a) hybrid Haar wavelet, (b) hybrid Daubechies 4 wavelet, (c) hybrid Coiflet 6 wavelet and (d) Input image.

The image quality measurement parameters PSNR & SSIM values for the varying fractional angle α are plotted in Fig 4.14 and Fig 4.15 respectively.

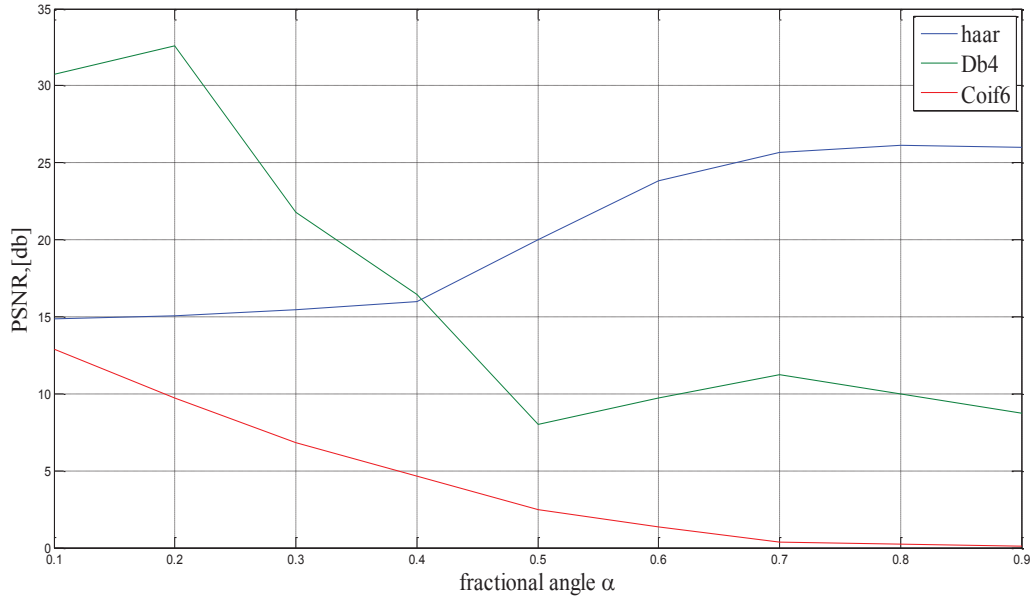

Fig 4.14: PSNR values for the reconstructed image plotted against the fractional angle for hybrid Haar, Daubechies 4 and Coiflet 6 wavelets

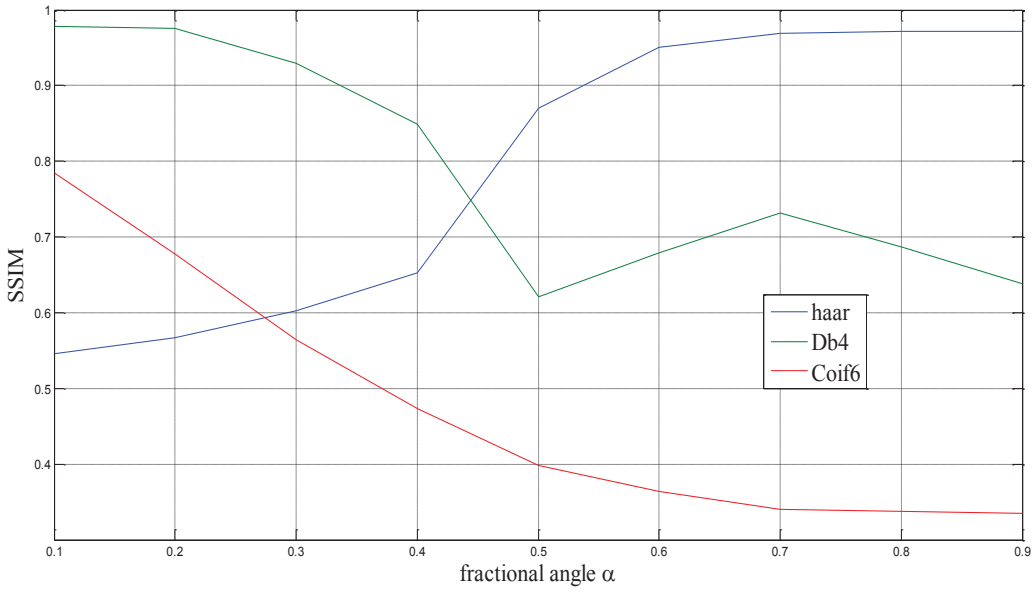

Fig 4.15: SSIM values for the reconstructed image plotted against the fractional angle for hybrid Haar, Daubechies 4 and Coiflet 6 wavelets

4.1.6 Application of the proposed method on the downsampled versions of the original image.

Case 1 – Input image size 128x128

The input image size was downsampled (from 256x256 pixels) to 128x128 pixels and the proposed method was repeated. The image quality measurement parameters PSNR & SSIM values for the varying fractional angle $'\alpha'$ are plotted in Fig 4.16 and Fig 4.17 respectively.

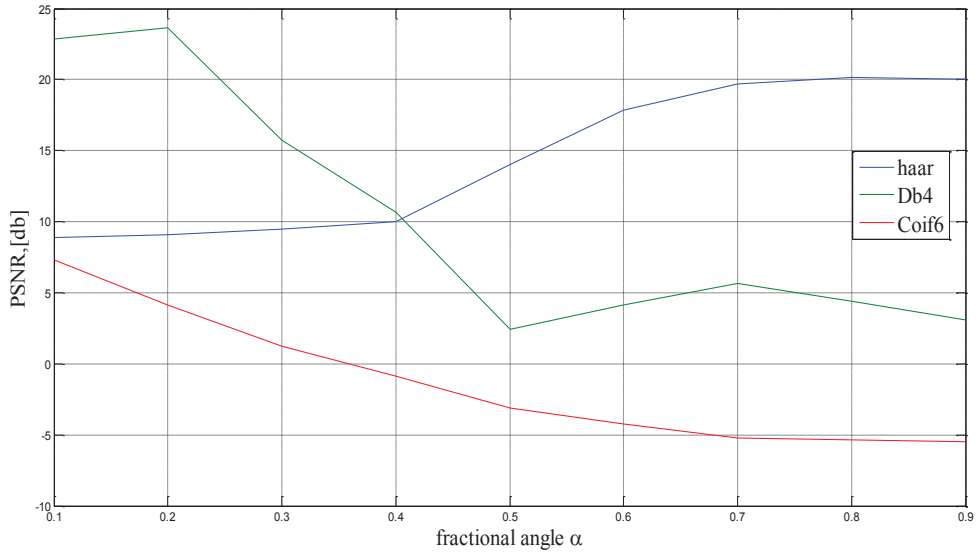

Fig 4.16: PSNR values for the reconstructed image of size 128x128 plotted against the fractional angle for hybrid Haar, Daubechies 4 and Coiflet 6 wavelets

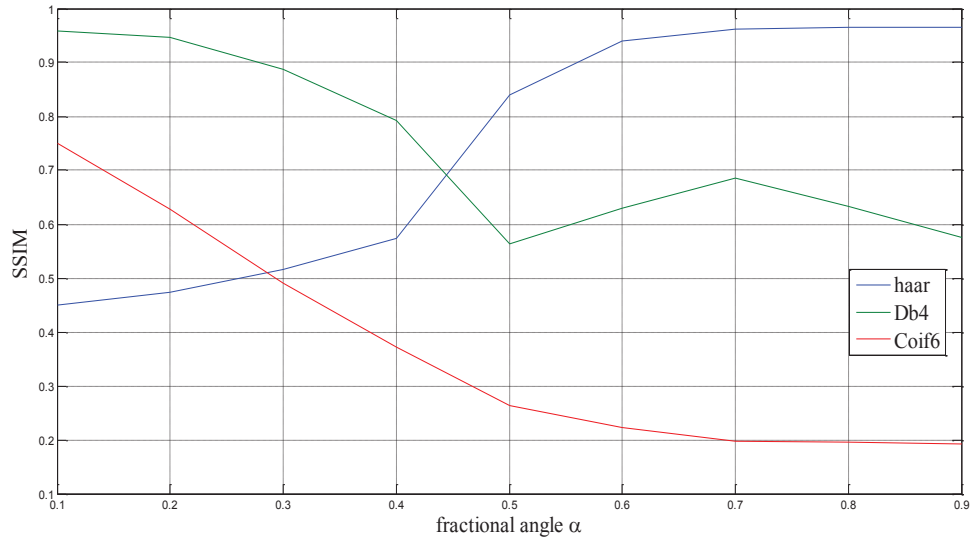

Fig 4.17: SSIM values for the reconstructed image of size 128x128 plotted against the fractional angle for hybrid Haar, Daubechies 4 and Coiflet 6 wavelets

Case 2 – Input image size 64x64

The input image size was downsampled (from 256x256 pixels) to 64x64 pixels and the proposed method was repeated. The image quality measurement parameters PSNR & SSIM values for the varying fractional angle $'\alpha'$ are plotted in Fig 4.18 and Fig 4.19 respectively.

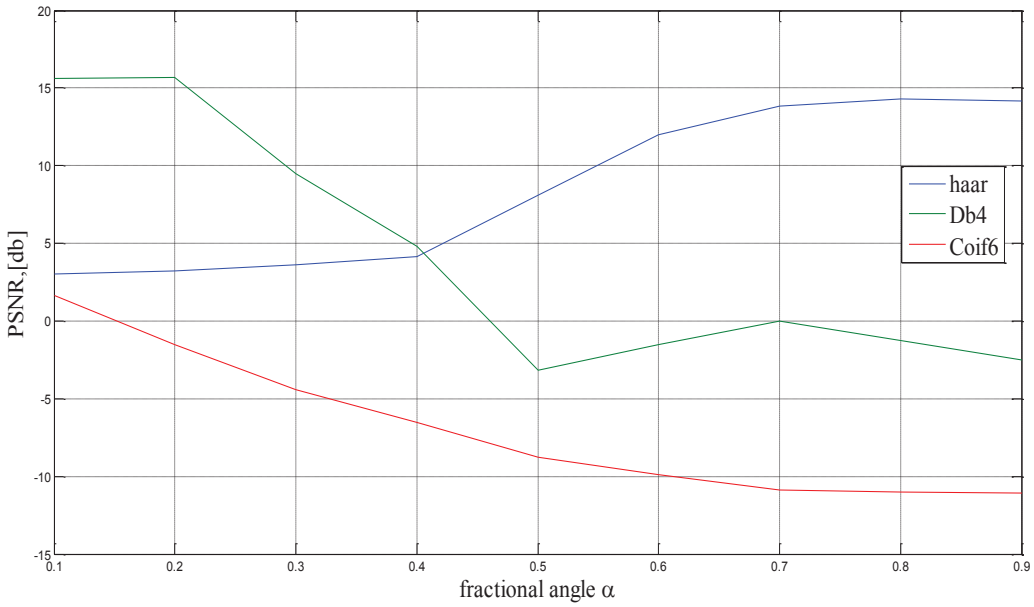

Fig 4.18: PSNR values for the reconstructed image of size 64x64 plotted against the fractional angle for hybrid Haar, Daubechies 4 and Coiflet 6 wavelets

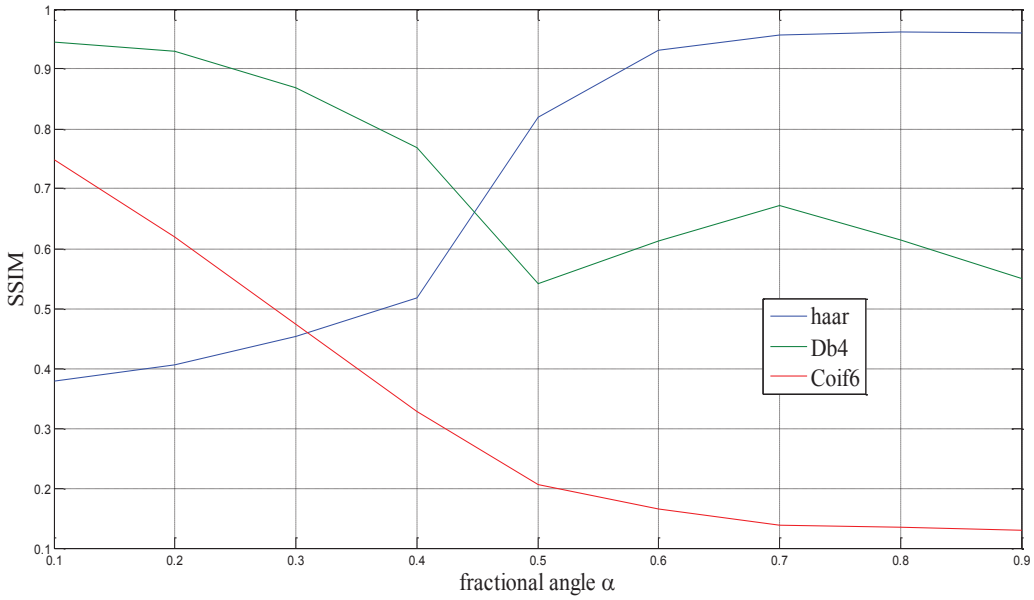

Fig 4.19: SSIM values for the reconstructed image of size 64x64 plotted against the fractional angle for hybrid Haar, Daubechies 4 and Coiflet 6 wavelets

4.1.7 Box plots for PSNR and SSIM:

The experiment results in sec 4.1.2 to 4.1.6 are acquired for a single image. In this section the set of PSNR and SSIM values for ten test images are represented in the form of boxplots.

Fig 4.20 shows the box plot of PSNR for Haar wavelet

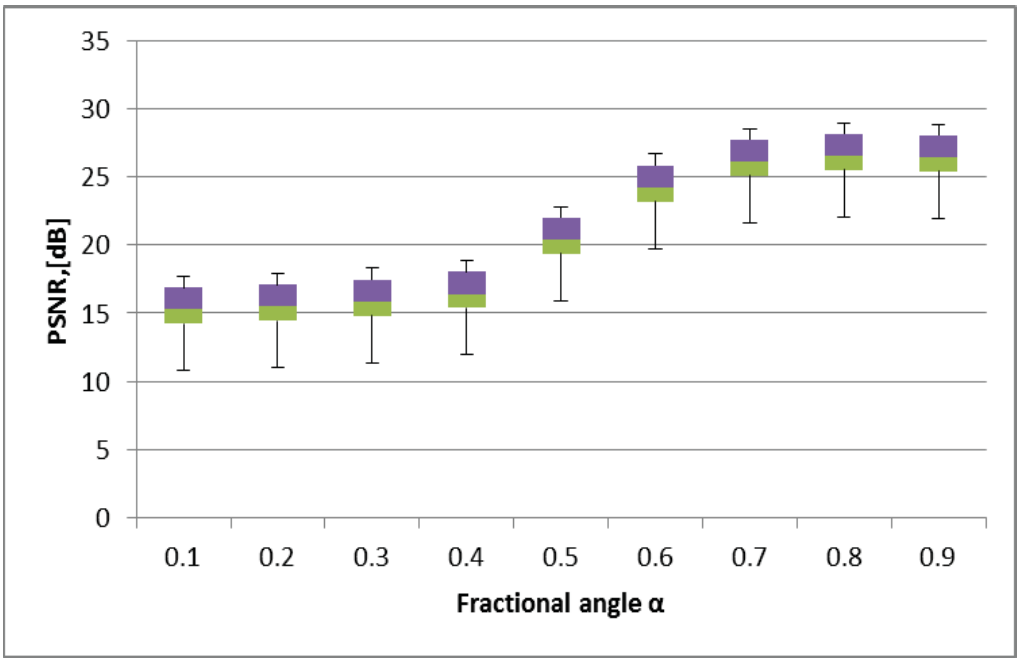

Fig 4.20 Box plot of PSNR for Haar wavelet

Fig 4.21 shows the box plot of SSIM for Haar wavelet

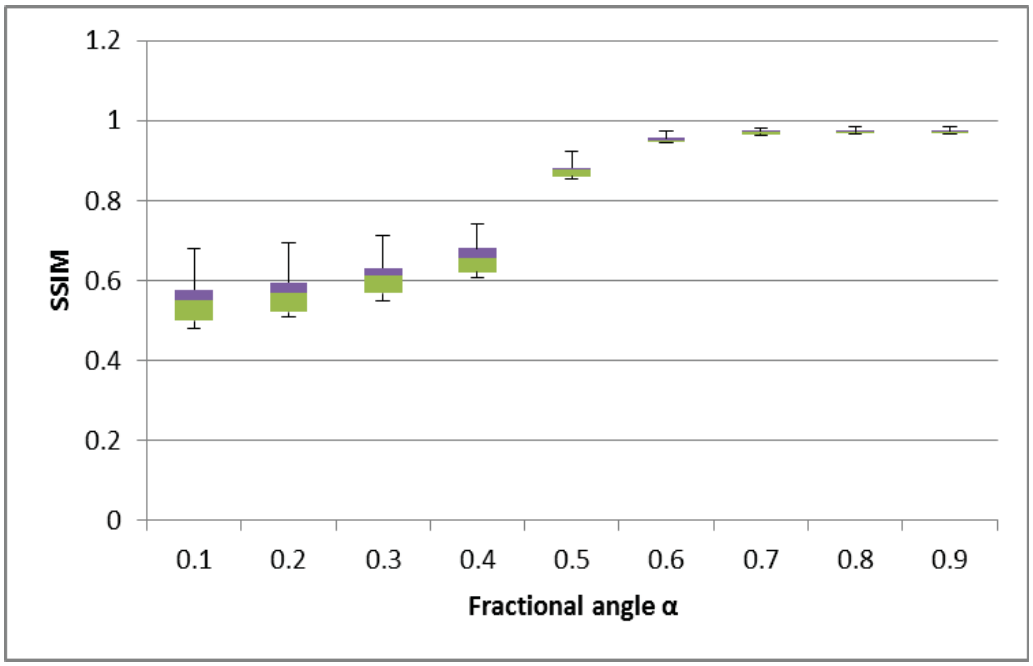

Fig 4.21: Box plot of SSIM for Haar wavelet

Fig 4.22 shows the box plot of PSNR for Daubechies 4 wavelet

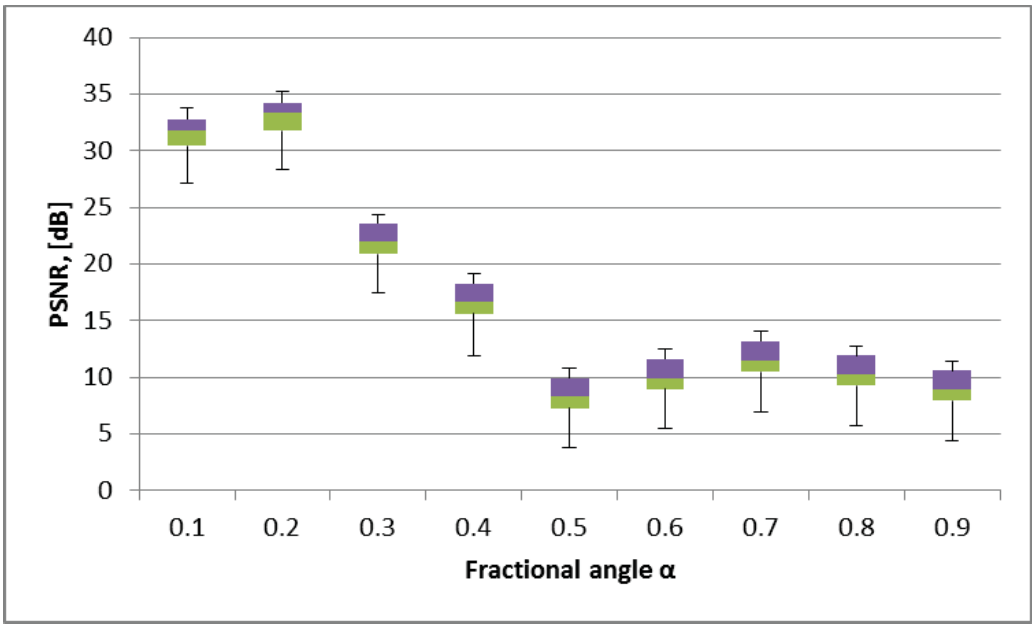

Fig 4.22: Box plot of PSNR for Daubechies 4 wavelet

Fig 4.23 shows the box plot of SSIM for Daubechies 4 wavelet

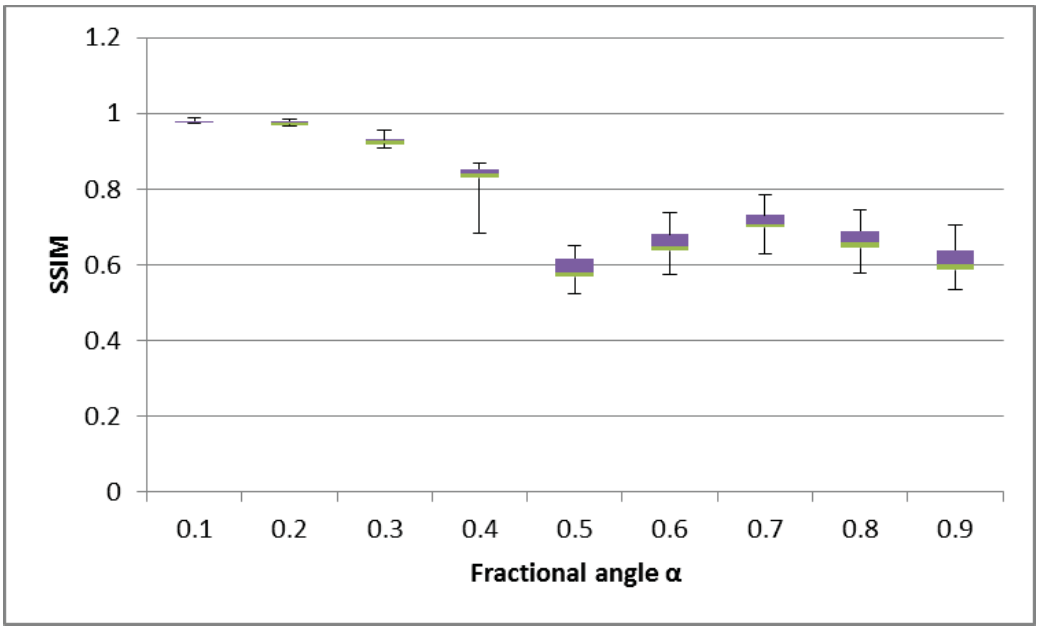

Fig 4.23: Box plot of SSIM for Daubechies 4 wavelet

Fig 4.24 shows the box plot of PSNR for Coiflet 6 wavelet

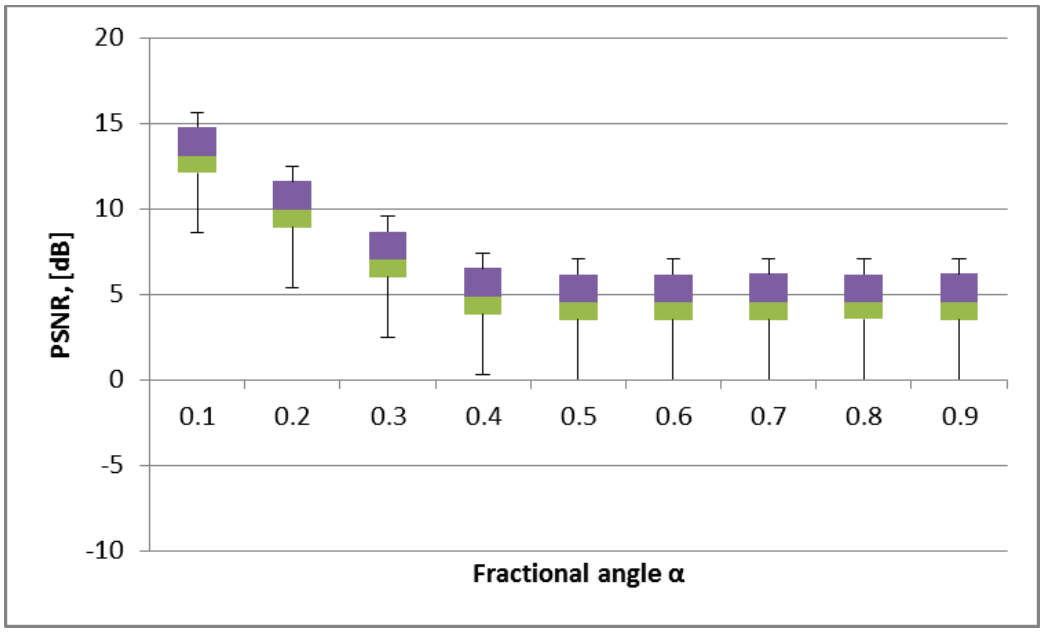

Fig 4.24: Box plot of PSNR for Coiflet 6 wavelet

Fig 4.25 shows the box plot of SSIM for Coiflet 6 wavelet

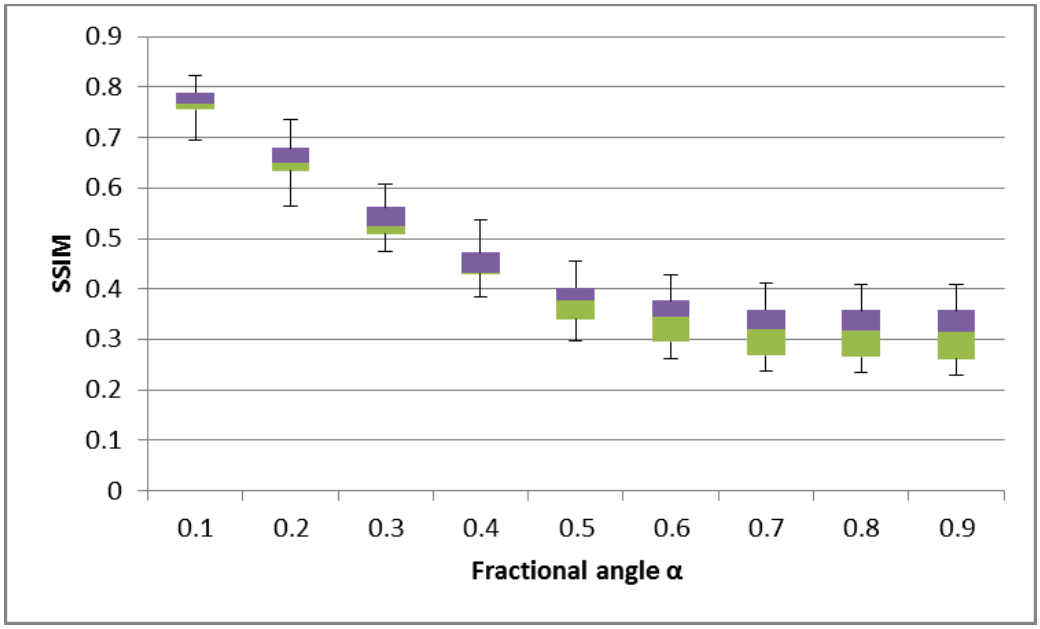

Fig 4.25: Box plot of SSIM for Coiflet 6 wavelet

4.2 Discussion

In our discussion the image reconstruction was carried out using Haar wavelet, Daubechies wavelet and Coiflet wavelets. The ideal values for SSIM and PSNR for a given wavelet are to be relatively high when compared to other wavelets for the better reconstruction. SSIM represents the similarity of the reconstructed imaged to the original image and must be ideally close to unity. Also PSNR represents the amount of signal and noise components in an image it must be positively high. A supplementary analysis was also done on 128*128 and 64*64 images to observe the performance of the wavelets.

In our analysis it was observed that the Daubechies has better performance in terms of PSNR for fractional angle $\alpha = 0.1\ to\ 0.4$ and Haar has better performance for fractional angle $\alpha = 0.4\ to\ 0.9$, compare blue and green plots in Figs. 4.14, 4.16 and 4.18. Coiflet has worst performance of the three analysed wavelets according to PSNR criteria, which can be observed in Figs 4.14, 4.16 and 4.18. However Daubechies out performs the other hybrid wavelets at $\alpha = 0.1\ to\ 0.25$.

Daubechies has better performance in terms of SSIM for fractional angle $\alpha = 0.1\ to\ 0.4$ and Haar has better performance for fractional angle $\alpha = 0.4\ to\ 0.9$, compare blue and green plots in Figs. 4.15, 4.17 and 4.19. Coiflet has worst performance compared to Daubechies and yields a slightly better result from $\alpha = 0.1\ to\ 0.25$ compared to Haar wavelet, which can be observed in Figs 4.15, 4.17 and 4.19. Based on the statistical analysis using box plots, the order of performance is given as

$$Daubechies\ 4\ wavelet > Haar\ wavelet\ \&\ Daubechies\ 4\ wavelet > Coiflet\ 6\ wavelet.$$

$$Haar\ wavelet > Coiflet\ 6\ wavelet.$$

$$i.e.,\quad Daubechies\ 4\ wavelet > Haar\ wavelet > Coiflet\ 6\ wavelet.$$

The above results are consistently true for the low resolution images also (64*64 and 128*128). But when compared them with the high resolution images, the performance of Low resolution images are low based on the depleted value of PSNR and SSIM. The main reason for this is attributed to the pixel stretching and loss of valuable data when the resolution of an image is reduced.

4.2.1 Boxplot analysis for PSNR and SSIM:

In a boxplot analysis of PSNR the lower and higher part of a plot gives the range of PSNR in each case. From the Figs 4.20, 4.22, 4.24 the maximum values of PSNR for Haar, Db4 and Coif6 wavelets are 28dB at $\alpha = 0.8$, 35dB at $\alpha = 0.2$ and 17dB at $\alpha = 0.1$ respectively. From the statistical analysis it clearly shows that Db4 produce the maximum PSNR performance at $\alpha = 0.1\ to\ 0.25$ on an average for ten images represented in the boxplot. The case is similar for SSIM since the upper and median values for SSIM are closer to unity for Db4 compared to that of Haar and coif6 wavelets.

Since the analysis is carried out for ten images instead of one image, we conclude that the results are consistent.

Chapter 5: Conclusion and Future Scope

5.1 Conclusion

In this thesis, we studied the image Reconstruction using wavelet transform with extended fractional Fourier transform. We focused on 3 kinds of wavelets namely Haar wavelet, Daubechies wavelet and Coiflets wavelet. These are the wavelets used to study the efficiency of the reconstruction algorithms.

The image quality parameters such as Structural Similarity Index Metric (SSIM) and Peak Signal to Noise Ratio (PSNR) are used to measure the efficiency of reconstructed image. From statistical analysis of results it can be concluded that Daubechies wavelet had the better performance compared to other wavelets at Fractional angle $\alpha = 0.1\ to\ 0.25$.

5.2 Future Scope

Our proposed method can be evaluated on different wavelets and results can be compared. Since each wavelet has its primary applications in beam forming, speech recognition, noise cancellation etc., the modified wavelet obtained by our proposed method can also be used for such applications.

Bibliography

[1].Herman, G. T., Fundamentals of computerized tomography: Image reconstruction from projection, 2nd edition, Springer, 2009

[2].Sirgurdur Helgason ,Radon Transform second edition Cambridge MA 1980

[3].Levoy, Marc. Volume rendering using the fourier projection-slice theorem. Computer Systems Laboratory, Stanford University, 1992.

[4].Xu, Minghua, and Lihong V. Wang. "Universal back-projection algorithm for photoacoustic computed tomography." Physical Review E 71.1 (2005): 016706.

[5].Doktor Ingeniur,Image Reconstruction from Fan-Beam and Cone-Beam Projections, University of Elangen, Germany 2008.

[6] Deng, Lanping, et al. "Efficient image reconstruction using partial 2D Fourier transform." Signal Processing Systems, 2008. SiPS 2008. IEEE Workshop on. IEEE, 2008.

[7] Tong, C. S., and K. T. Leung. "Super-resolution reconstruction based on linear interpolation of wavelet coefficients." *Multidimensional Systems and Signal Processing* 18.2-3 (2007): 153-171.

[8] Zhang, Yan, Yuanyuan Wang, and Chen Zhang. "Efficient discrete cosine transform model–based algorithm for photoacoustic image reconstruction."*Journal of biomedical optics* 18.6 (2013): 066008-066008.

[9] Verma, Rohit, et al. "A Novel Image Reconstruction Using Second Generation Wavelets." *Advances in Recent Technologies in Communication and Computing, 2009. ARTCom'09. International Conference on*. IEEE, 2009..

[10] Azeez, Hadeel Ali, and Saad Ali Amin. "Medical Image Reconstruction Using Wavelets and Multi-Wavelet Methods." *Developments in E-systems Engineering (DeSE), 2011*. IEEE, 2011.

[11] Chen, Huawei, Ichiro Hagiwara, and A. Kiet Tieu. "Image reconstruction based on combination of wavelet decomposition, inpainting and texture synthesis."*International Journal of Image and Graphics* 9.01 (2009): 51-65.

[12].James S. Walker, “A Primer on Wavelets and their Scientific Applications”, 2nd ed., 2008.

[13].P.Sivakrishna, A.B.Moghul. “Super Resolution Image Reconstruction using LWT”, Blekinge Institute of technology”, 2012.

[14]. http://users.rowan.edu/~polikar/WAVELETS/WTpart4.html.

[15]. Soman, K. P., and K. I. Ramachandran. *Insight Into Wavelets From Theory To Practice 2Nd Ed*. PHI Learning Pvt. Ltd., 2005.

[16]. Wei, Dong, Alan C. Bovik, and Brian L. Evans. "Generalized coiflets: a new family of orthonormal wavelets." *Signals, Systems & Computers, 1997. Conference Record of the Thirty-First Asilomar Conference on*. Vol. 2. IEEE, 1997.

[17]. Kumar, S. Suresh, and H. Mangalam. "Wavelet-based Image Compression of Quasi Encrypted Grayscale Images." *International Journal of Computer Applications* 45 (2012).

[18]. Sandeep , Gaganpreet , Dr.Dheerendra Singh, "Comparative Analysis of Haar And Coiflet Wavelets using Discrete Wavelet Transform In Digital Image Compression", 2012 Vol. 2,Issue 2,pp.669-672.

[19]. I.Samil Yetik, M. Alper Kutay, Haldum M.Ozaktas, "The Fractional Fourier Transform and Its Applications to Image Representation and Beamforming", 2002.

[20]. Shi, Jun, NaiTong Zhang, and XiaoPing Liu. "A novel fractional wavelet transform and its applications." *Science China Information Sciences* 55.6 (2012): 1270-1279.

[21].Walker, James S. "Fourier analysis and wavelet analysis." Notices of the AMS44.6 (1997): 658-670.

[22].Kumar, Naveen, and B. Venu Gopal. "VLSI Implementation of Data Encryption Standard Algorithm.",2012.

[23]. Sanna Jäälinoja, "Aspects of Cryptography and Internet Security", 1999.

[24]. Jayaraman, S., Esakkirajan, S. and Veerakumar, T. Digital Image Processing,Tata

McGraw Hill Education Private Limited, India, 2009.

[25]. Z. Wang, A. C. Bovik, H. R. Sheikh, and E. P. Simoncelli, "Image quality assessment: From error visibility to structural similarity," *Image Processing, IEEE Transactions on*, vol. 12, no. 4, pp. 600–612, 2004.